TRIBHUVAN UNIVERSITY
INSTITUTE OF ENGINEERING
PULCHOWK CAMPUS

THESIS NO: 079MSMSE001

Preparation of Activated Carbon from Jacaranda Seed Pods as Anode Material in Supercapacitors

by

Ashman Karki

A THESIS

SUBMITTED TO THE DEPARTMENT OF APPLIED SCIENCES AND CHEMICAL ENGINEERING

IN PARTIAL FULFILLMENT OF THE REQUIREMENTS FOR THE

DEGREE OF MASTER OF SCIENCE IN MATERIAL SCIENCE AND ENGINEERING

DEPARTMENT OF APPLIED SCIENCES AND CHEMICAL ENGINEERING
LALITPUR, NEPAL

MAY, 2025

COPYRIGHT

TRIBHUVAN UNIVERSITY
INSTITUTE OF ENGINEERING
PULCHOWK CAMPUS
DEPARTMENT OF APPLIED SCIENCES AND CHEMICAL ENGINEERING

The undersigned certify that they have read, and recommended to the Institute of Engineering for acceptance, a thesis entitled **"Preparation of Activated Carbon from Jacaranda Seed Pods as Anode Material in Supercapacitors"** submitted by Ashman Karki (079MSMSE001) in partial fulfilment of the requirements for the degree of Masters in Material Science and Engineering.

Assistant Professor Dr. Tanka Mukhiya
Supervisor
Department of Applied Sciences and Chemical Engineering
Institute of Engineering, Pulchowk Campus
Tribhuvan University

Professor Dr. Meena Rajbhandari
External Examiner
Research Centre For Applied Science And Technology (RECAST)
Tribhuvan University

Professor Dr. Sahira Joshi
Head of Department
Department of Applied Sciences and Chemical Engineering
Institute of Engineering, Pulchowk Campus
Tribhuvan University

ABSTRACT

The global energy crisis focuses on utilizing sustainable, eco-friendly, and cost-efficient alternatives to traditional energy storage systems. The tunable porosity, large surface area, and excellent cyclic stability have made biomass-derived activated carbon - a promising electrode material for supercapacitor applications. The thesis presents a novel approach to the synthesis of AC from Jacaranda Seed Pods (JSP) – a lignocellulosic biowaste- via phosphoric acid (H_3PO_4) activation followed by carbonization at 850 °C and 900 °C in an atmosphere of nitrogen.

Under physicochemical characterization, Fourier Transform Infrared Spectroscopy (FTIR) indicated proper carbonization and X-ray Diffraction (XRD) revealed the amorphous nature of activated carbon, turbostratic disordered carbon structure, and partial graphitic domains with sp^2 hybridization within the carbon matrix. Further, the Field Emission Scanning Electron Microscope with Energy Dispersive Spectra (FESEM with EDX) showed a well-developed micro-mesoporous framework with carbon as a chief element. Additionally, under electrochemical evaluation in a three-electrode system, the Cyclic Voltammetry (CV) curve displayed a quasi-rectangular shape which verified the formation of the electric double-layer (EDLC) type supercapacitor for both ACJSP-850 and ACJSP-900. Similarly, Electrochemical Impedance Spectroscopy (EIS), and Galvanostatic charge-discharge (GCD) curves reflected the electrode behavior at different frequencies, and current densities respectively. As-prepared ACJSP-900 demonstrated better performance with a specific capacitance of 182 F g^{-1} at 1 A g^{-1} compared to 120 F g^{-1} in ACJSP-850 at 1 A g^{-1}. The superior performance of ACJSP-900 was attributed to enhanced graphitization, higher diffusion rates, lower electrolyte resistance, and lower charge transfer resistance (R_s = 0.67 Ω, R_{ct} = 0.46 Ω).

As far as we are aware, this is the first research on AC prepared by Jacaranda Seed Pods studying electrochemical behavior and energy storage applications. The results highlight the viability of using AC from lignocellulosic biomass - JSP as a sustainable, economical, and efficient electrode material.

Keywords: Activated carbon, lignocellulosic biowaste, turbostratic, graphitization, chemical activation, energy storage

ACKNOWLEDGEMENTS

It gives me immense pleasure to express my gratitude to my supervisor Assistant Professor Dr. Tanka Mukhiya from the Department of Applied Sciences and Chemical Engineering, Pulchowk Campus, Tribhuvan University for their suggestions, guidance, and motivation for conducting and completion of my thesis work.

I am also grateful to Assistant Professor Deval Prasad Bhattarai, Assistant Professor Prakash Chandra Lohani, and Assistant Professor Khem Raj Shrestha for their advice and mentorship. Further, I would like to thank all the faculty members, lab technicians, and department staff for making this research smooth.

Additionally, I would like to acknowledge my colleagues Ms. Bipana Ojha Khatri, Mr. Gyanendra Pal, Mr. Saugat Chapagain, and Mr. Bibek Ghimire for their constructive feedback, and technical support throughout the journey.

My highest recognition and deepest praise to my family for inspiring, and encouraging me onto my thesis completion. Their faith and patience have always been a source of strength towards my thesis completion. I owe this to them.

TABLE OF CONTENTS

LIST OF TABLES

LIST OF FIGURES

LIST OF ABBREVIATIONS AND SYMBOLS

Abbreviations	
AC	Activated Carbon
ACJSP-850	Activated Carbon Jacaranda Seed Powder @ 850 °C
ACJSP-900	Activated Carbon Jacaranda Seed Powder @ 900 °C
BET	Brunauer-Emmett-Teller
BJH	Barrett-Joyner-Halenda
CV	Cyclic Voltammetry
EDLC	Electric Double-Layer Capacitor
EIS	Electrochemical Impedance Spectroscopy
EDX	Energy Dispersive Spectra
FTIR	Fourier Transform Infrared Spectroscopy
FESEM	Field Emission Scanning Electronic Microscopy
GCD	Galvanostatic Charge Discharge
IR	Impregnation Ration
JSP	Jacaranda Seed Pods Powder
TGA	Thermogravimetric analysis
XRD	X-ray Diffraction
Symbols	
$A\ g^{-1}$	Ampere per gram
C	Capacitance
°C	Degree Celsius
$°C\ min^{-1}$	Degree Celsius per minute
$F\ g^{-1}$	Farad per gram
g	gram
h	hour
ml	milliliter
$mV\ s^{-1}$	millivolt per second
nm	nanometer
R_s	Solution Resistance
R_{ct}	Charge Transfer Resistance
Wo	Warburg Impedance
Z	Impedance
Z’	Real part of Impedance
Z”	Imaginary part of Impedance

CHAPTER 1: INTRODUCTION

1.1 Background

The development of modern technologies like electronics, electric vehicles, smartphones, infrastructures, etc. has made a significant impact on human lives. These lead to the higher consumption of energy sources like oil, coal, and natural gases. Though sustainable approaches like wind, solar, and hydropower have been prominent, the intermittence and reliability of these sources always remain a global concern (Farghali et al., 2023). Thus, the need for advanced and sustainable energy storage systems has captured interest recently. Energy storage devices like batteries have high energy densities but aren't holding up due to their low power density and cyclic stability. Supercapacitors- electrochemical energy storage devices- progressed their way due to their high-power density, longer operational life, fast charging-discharging, and limiting environmental impact (Libich et al., 2018).

Offering high power density with moderate energy density, supercapacitors are electrochemical energy storage devices that hold the properties of capacitors and batteries. The mechanism involves the electrostatic charge accumulation at the electrolyte-electrode interface forming an electric double-layer capacitor or exhibiting a fast redox reaction for pseudo-capacitor formation (Salanne et al., 2016).

Activated carbon is a low-cost, highly porous carbonaceous material that can be tailored to increase its surface area and adsorption capacity for various water treatment, air purification, and energy storage applications (Heidarinejad et al., 2020). Under aberration-corrected transmission and field emission scanning electron microscopy, activated carbon exhibits a graphene-like stacking, turbostratic, amorphous carbon structure, which explains its microporosity, enhanced conductivity through graphitization (Harris et al., 2008). When a carbon material undergoes structural modification via functionalization, metal or oxide deposition, etc., it is known as activated carbon; however, if the carbon is categorized by its physiological properties such as large surface area, pore size, and low density, it is known as porous carbon. Activated carbon is a technically porous carbon, but not all porous carbons can be identified as activated carbon (Gan, 2021).

While coal is considered a major source of AC, other sources are lignocellulosic biomasses, wood, and, animal wastes (Iwanow et al., 2020). Among them, lignocellulosic biomass is characterized as an eco-friendly, cost-effective, and abundantly found material on the earth. Thus, activated carbon can be produced from these materials. Because of their highly porous nature and good adsorption capacity, these biomasses could resort to wastewater treatment and air purification with the least environmental impact (Iwanow et al., 2020).

Various studies on underutilized and abundant biomass sources have been carried out to study the potential applications of activated carbon in different materials, particularly electrodes in supercapacitors and wastewater treatments, focusing on its surface area, eco-friendliness, porous nature of activated carbon, conductivity, and thermal stability with optimized physicochemical properties (Cheng et al., 2020; Ullah et al., 2024).

Figure 1 *Jacaranda mimosifolia Plant and its seed pods*

This paper focuses on employing seed pods from *Jacaranda mimosifolia* trees as a potential source of activated carbon. *Jacaranda mimosifolia* belonging to the Bignoniaceae family are semi-evergreen deciduous trees with blue flowers originally from the South American region (Aguirre-Becerra et al., 2020) . The plants are now

widespread in various tropical regions of Australia, South Africa, North America, and South Asia. These *Jacaranda mimosifolia* trees are also widely found in Nepal. For several periods, they were known as lignocellulosic biomass with minimum utilization and no application. Jacaranda seeds, like other biomasses, contain cellulose, hemicellulose, and lignin, which determine the presence of carbon in the material (Jiang et al., 2020; Li et al., 2016; Nor et al., 2013).

Activated carbon prepared from Jacaranda Seed Pods have been tested for various applications like Aqueous-phase ketoprofen removal (Georgin et al., 2021), removal of heavy metals (Valdés-Rodríguez et al., 2022), dyes (Treviño-Cordero et al., 2013), and in mercury adsorption (Morales-Herrera et al., 2024). However, further studies on Jacaranda seed pods as activated carbon materials and their potential in energy storage are yet to be explored and recognized.

Among the various applications of activated carbon (AC), biomass-derived AC has made its way towards a sustainable and efficient medium for energy storage, typically a supercapacitor. The characteristics such as high specific surface area, tunable porosity, cyclic stability, electrical conductivity, etc. make it distinguished as an electrode material for electric-double layer capacitors as well as hybrid supercapacitors (Saini et al., 2021). Furthermore, biowaste like coconut shells, sugarcane bagasse, sawdust, etc. as a precursor lowers the production cost as well as addresses global environmental concerns (Owsianiak et al., 2021).

AC properties such as pore structure and surface functionality can be tailored with different activation techniques mainly, physical and chemical activation. They also create a significant influence on ion diffusion rate and charge storage thus overall enhancing the electrochemical performance.(Niya & Andrews, 2022). Relatively, heteroatom doping and surface modification can further revamp its conductivity and specific capacitance leading to high-performance energy storage devices (Kumar et al., 2020).

Since green circular economy principles have been trending, the AC prepared from biomass aligns with the green route for eco-friendly and scalable electrode materials. Thus, the motivation for employing Jacaranda Seed Pods is to identify novel biomass sources, encourage and enhance the green circular economy by reducing these

biowastes, and get into the in-depth electrochemical behavior, the porous carbon structures formations, and their interrelationships.

The activated carbon from Jacaranda Seed Pods (JSP) gives a perception of phosphoric acid activation on JSP biomass, investigates the electrode performance as an electric double-layer capacitor, its specific capacitance, diffusion characteristics, charging-discharging behavior, potential surface functionalization, equivalent circuit formation, as well as its structural and surface properties relationships.

1.2 Methods of Activation

Carbon activated as a material with high porosity and a wide surface area is an exceptional adsorbent for different uses such as charge storage, purifying water, cleaning air, and storing gas. The activation process, where volatile matter is carefully removed and a porous structure is created, is what gives it its distinctive characteristics. Carbon activation can be done through various methods.

1.2.1 Physical Activation

Physical activation comprises the carbonization of a carbon-containing precursor, succeeded by a gasification process (Rodríguez-Reinoso & Molina-Sabio, 1992). The gasification procedure usually involves the use of steam, carbon dioxide, or a combination of the two, at elevated temperatures (700-1000°C). Gasification agents react with the precursor's carbon to form pores.

- Steam activation: These type of activation utilizes steam where it reacts with the carbon to produce carbon monoxide and hydrogen (Molina-Sabio et al., 1996).
- Carbon dioxide activation: This method produces a carbon with a higher degree of microporosity compared to steam activation as it creates more microporosity in activated carbon while steam activation widens microporosity and produces lower micropore volume (Molina-Sabio et al., 1996).
- Mixed gas activation: A combination of steam and carbon dioxide can be used to achieve a desired pore structure in the activated carbon (Chen & Lin, 2013).

1.2.2 Chemical Activation

Chemical activation requires treating the carbonaceous precursor with a chemical agent before carbonization. The chemical compound works as a dehydrating agent or a catalyst, aiding in the creation of pores while carbonizing. Zinc chloride, sodium

hydroxide, potassium hydroxide, phosphoric acid, and sulfuric acid are some typical chemical activating agents.

- Salt activation: The hygroscopic prepare includes salts with a tall partiality for water drawing dampness from wet carbon antecedents, encouraging lack of hydration, which upgrades carbonization productivity, makes strides pore structure, increments adsorption capacity, and decreases generation costs within the planning of enacted carbon (Głowniak et al., 2021).
- Bases activation: The bases response forcefully responds with carbon, essentially breaking down its structure to form pores with a tall surface zone (J. Chmiola et al., 2006).
- Acid activation: Acid activation involves through the method of proton exchange, hydrogen particles (H^+) are given to the oxygen particle in water atoms, coming about within the arrangement of hydronium particles (H_3O^+) and breaking the O-H bond (Zhao & Liu, 2021).

1.3 Phosphoric Acid Activation: Mechanism and Relevance

Chemical activation through phosphoric acid involves the process of dehydration, crosslinking with polymer fragments forming phosphate esters, and polyphosphate bridges, mesopores and micropores formation, and further elimination of phosphorous compounds (Suárez-Garcıa et al., 2002).

The activation mechanism of phosphoric acid at various temperatures:

100 – 400°C: Removal of water molecules, and formation of polyphosphoric acid compounds.

$2H_3PO_4 \rightarrow H_4P_2O_7 + H_2O$ ……. (i)
$3H_3PO_4 \rightarrow H_5P_3O_{10} + 2H_2O$…… (ii)
$nH_3PO_4 \rightarrow H_{n+2}P_nO_{3n+1} + (n - 1)\ H_2O$ ……. (iii)

400 – 700 °C: Polyphosphoric acid dehydration forms phosphorous pentoxide which further reacts with carbon forming different pore structures, thus releasing carbon dioxide. Also, the surface functional groups release carbon monoxide in reaction with phosphorous pentoxide.

$H_{n+2}P_nO_{3n+1} \rightarrow P_4O_{10} + H_2O$…… (iv)
$P_4O_{10} + 2C \rightarrow P_4O_6 + 2CO_2$ …… (v)

700 – 800 °C: Production of phosphine gas when reaction with hydrocarbon occurs. Also, the release of byproducts like CO and CO_2 might take place.

P_4O_{10} or $P_4O_6 + CH_x \rightarrow PH_3 + CO_2$ or CO……. (vi)

Above 800°C: Phosphorous compounds evaporate leaving behind a large number of pores. The different pore sizes formed helps to enhance the ion conductivity, charge storage, and decrease the charge resistance inside the prepared activated carbon (Li et al., 2015; Neme et al., 2022).

Phosphoric acid activation is a controlled process. It avoids over-itching and pore collapse, helping the distribution of mesopores and micropores. Additionally, the phosphorous compounds are water soluble making post-treatment easier (El Hadrami et al., 2022).

1.4 Structural and Surface Characteristics of Activated Carbon

Structural properties like porosity, pore size distribution, specific surface area, graphitization, and the presence of different functional surface groups play a critical role in the performance of AC (Zhang et al., 2022). The highly porous AC has a high adsorption capacity as well as it boosts its specific capacitance. Further, the distribution of mesopores and micropores inside the porous AC is also a significant factor. High micropores volume is effective for gas adsorption, and small molecule capture, and increases the overall surface area of AC for ion adsorption. The mesopores present are useful for liquid-phase adsorption of larger contaminants, and facilitate the ion transport, reducing internal resistance and thus improving power density (Yu et al., 2017). Similarly, the specific surface area in AC determines it adsorption capacity, and number of active sites present for charge storage. A higher surface area signifies more active sites for gases, liquids and solutes entrapping. This also means more ions adsorb form the electrolyte and thus energy density increases. However, the low small pores (nanopores) hinder the whole charge storage mechanism (Li et al., 2024).

The sp^2 hybridization within the carbon matrix incorporates the partial graphitization of AC. This helps to enhance the conductivity and electrochemical properties (Wang et al., 2022). Additionally, the presence or doping of different functional groups like hydroxyl, carboxyl, carbonyl, nitrogen doping etc. contributes in the pseudocapacitive nature of the AC optimizing the electrochemical behavior (Liu et al., 2015).

1.5 Fundamentals of Supercapacitors

As the technology is advancing a lot of people are inclined using different electronic devices. These devices like EV cars, Smart Watches, mobile phones, laptops, etc. need different electrochemical devices for energy storge and its operation. Among them, supercapacitor gained its popularity due to its high-power density, rapid charging-discharging property, and cycling stability. The electrolyte and electrode material determines the characteristics and electrochemical properties of the supercapacitor (Libich et al., 2018). Based on the property of supercapacitor they are divided into three types:

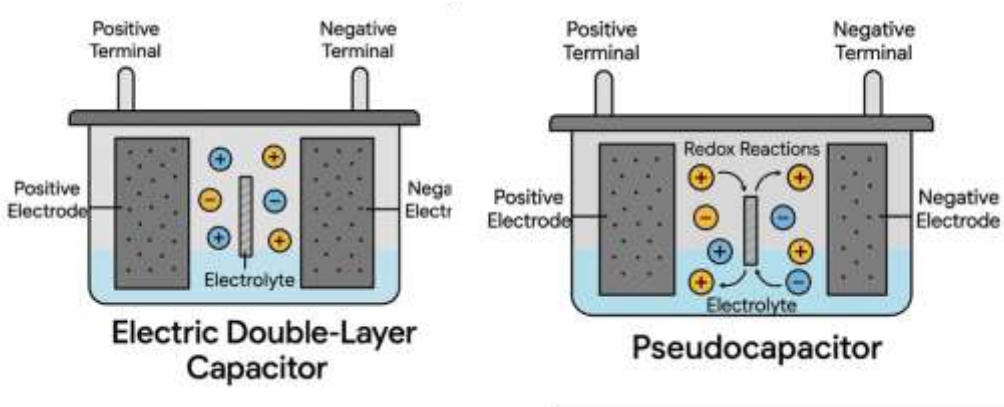

Figure 2 *Different types of Supercapacitors*

1.5.1 Electrochemical Double-Layer Capacitors (EDLCs)

These utilize the formation of Helmholtz double layers due to electrostatic force between the ions at the electrode-electrolyte interface, where charge separation happens devoid of faradaic reactions. Employing carbonaceous materials with high specific surface areas, such as activated carbon, graphene, or carbon aerogels, EDLCs demonstrate excellent power density and swift charge-discharge kinetics, yet they are limited by lower energy density (Libich et al., 2018).

1.5.2 Pseudo capacitors

Distinguished by rapid and reversible faradaic charge transfer, these supercapacitors utilize redox-active substances like transition metal oxides (e.g., RuO_2, MnO_2) and conductive polymers. The occurrence of rapid redox reactions at the electrode interface notably increases specific capacitance relative to EDLCs, though it may involve potential compromises in cyclic stability and rate performance (Bhojane, 2022).

1.5.3 Hybrid Supercapacitors

Hybrid supercapacitors cleverly combine the high-power density of electrochemical double-layer capacitors (EDLCs) with the improved energy density from faradaic redox reactions, utilizing asymmetric electrode designs. By merging carbon-based substances with pseudocapacitive or battery-like electrodes—commonly employing transition metal oxides or conductive polymers—they attain enhanced charge storage abilities. This collaboration facilitates quick ion movement, reduced internal resistance, and prolonged cycle lifespan, making them crucial for the future of energy storage in electric transport and grid stability. Fundamentally, they connect rapid charge dynamics with extended energy storage(Chatterjee & Nandi, 2021).

1.6 Charge Storage Mechanism in Electric Double Layer Capacitors (EDLCs)

The ionic behavior at the surface of the electrode in an electrochemical double-layer capacitor (EDLC) has been explained by several classical models. These models describe the organization of ions within the electrode-electrolyte interface.

1.6.1 Helmholtz Model

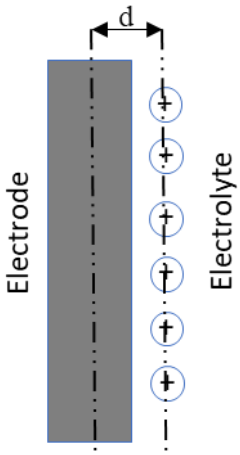

Figure 3 *The Helmholtz Layer*

The Helmholtz model of the 19th century explained the electric double-layer concept between electrode and electrolyte. According to this concept, the electrode and electrolyte develop two opposite charges and are separated by a distance d (Fig 3) to form an electric double layer (Helmholtz, 1853). However, the ions in real systems aren't ideally placed and can drift as a result of thermal energy.

1.6.2 Gouy-Chapman Model

The Gouy-Chapman model then developed Helmholtz's idea by adding the effect of thermal agitation. Ions are not taken to be in a dense solid layer but are instead assumed to be diffusely distributed around the electrode surface (Gouy, 1910; Chapman, 1913). Ion concentration is exponentially related to distance from the electrode as defined in this model. The diffuse layer of ions has a lower capacitance than the dense Helmholtz layer (Gouy, 1910). The large thickness prediction of a double layer at large surface charge densities makes this model somewhat less reliable since capacitance is underestimated.

1.6.3 The Stern Model

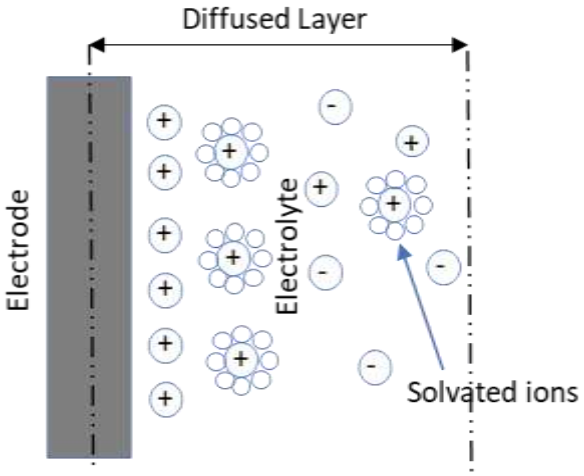

Figure 4 *The Stern Model*

Both the Helmholtz layer (C_h) and the diffusion layer (C_d) are present in the electric double layer capacitor, which is the main idea of the Stern model (Stern, 1924). Thus, the total capacitance (C_o) is:

$$C_o = \frac{1}{C_h} + \frac{1}{C_d} \quad \text{..... (1)}$$

1.6.4 Grahame Model

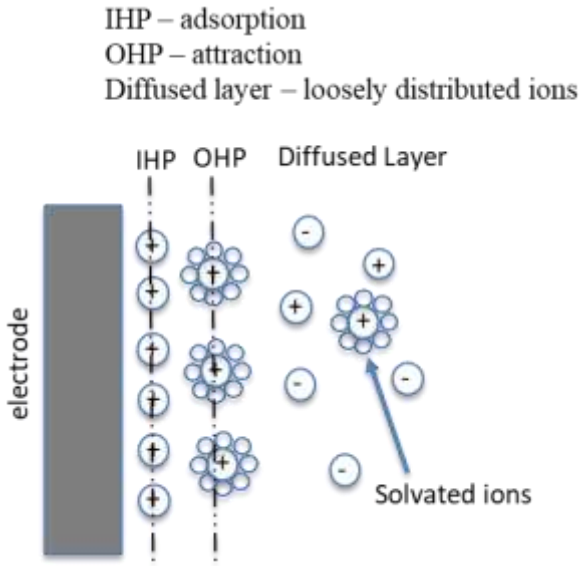

Figure 5 *Grahame Model*

The stern model was further modified where the Helmholtz plane was further divided into the Inner Helmholtz Plane (IHP), and Outer Helmholtz Plane (OHP). The IHP passed through the adsorbed ions center while OHP passed through the center of solvated ions (Grahame, 1947).

1.7 The Electrodes and Electrolytes in Supercapacitors

1.7.1 The Electrodes

In Electrochemical Double-Layer Capacitors (EDLCs), the electrode material plays a vital role because it directly affects the storage capacity and also its performance. They hold the charge by permitting ions in the electrolyte to stick on their surface whenever voltage is supplied. Therefore, the electrode material is important. It must have an enormous surface area so ions can stack up more, and that means there can be a lot more energy stored.

Activated Carbon is the most widely used electrode material because it's cheap, widely available, and possesses a very high surface area — sometimes over 1000 square meters per gram (Simon & Gogotsi, 2008). Activated carbon is usually derived from some sort of natural material like coconut shells or wood, which are then heated and processed to become very porous.

For high-end applications, scientists use materials like carbon nanotubes (CNTs) and graphene. They are peculiar carbon structures where the carbon atoms are held in highly

ordered arrangements. They enable ions to move faster and make the device charge and discharge more quickly (Zhang & Zhao, 2009). Their disadvantage is that they are extremely costly and, thus are not yet commonly used in standard supercapacitors.

There are carbon nanofibers and carbon aerogels, too. They create networks of extremely fine pores through which the ions are able to freely pass, which is better in how rapidly the device can work. Researchers have been known to mix two distinct types of carbon material for even superior performance.

1.7.2 The Electrolytes

An electrolyte is a compound which when it is dissolved in a solvent like water or at times organic solvents releases ions. It is the ions that render the material conductive. When talking of energy storage systems like EDLCs, batteries, and fuel cells, electrolytes play a crucial function of transporting a charge between both electrodes when charging or discharging is taking place.

When a voltage is applied between an EDLC, the cations move toward the negatrode and the anions are attracted towards the positrode. This movement of ions in electrolytes thus directly corelates with the flow of electrons in the external circuit. The performance of an EDLC or battery depends upon a good electrolyte.

Electrolytes may be

i. Water Electrolytes (potassium hydroxide, sulfuric acid): They provide good ionic conductivity but a narrow voltage window of about 1.0 V owing to water degradation (Conway, 2013).
ii. Organic Electrolytes (acetonitrile-based): They allow high voltage with range between 2.5-3.0 V, with higher energy density but lowered conductivity and safety concerns (Simon & Gogotsi, 2008).
iii. Ionic Liquid Electrolytes: They offer even higher voltage operation and thermal stability, and typically more expensive and more viscous (Zhang & Zhao, 2009).

The electrolyte directly impacts the voltage capacity of the EDLC, energy, and power density, internal resistance, and life span. Therefore, the electrolyte should possess high conductivity, wide electrochemical stability, good potential window, and be cheaper.

1.8 Activated Carbon as an Electrode Material

The large surface area, remarkable conductivity, and affordability of Activated Carbon (AC) makes it one of the most commonly electrode material in electric double-layer capacitors (EDLCs) formation. In EDLCs, energy is stored through the electrostatic adsorption of ions at the interface of the electrolyte and the porous carbon electrode, creating a double layer without faradaic reactions, facilitating fast charge-discharge cycles and a long operational lifespan (Conway, 2013).

The pore architecture and surface properties determine the efficiency of AC as a supercapacitor. Mesopores (2–50 nm) promotes ion transportation and lowers resistance while, Micropores (pores <2 nm) increases the charge storage capacity by offering a vast surface area for ion adsorption (Simon & Gogotsi, 2008). Generally, specific capacitance of AC reaches from 100 to 300 F/g, depending on the electrolyte and material synthesis technique (Pandolfo & Hollenkamp, 2006). Surface functionalization from oxygen- or nitrogen-containing groups further enhances wettability and ion accessibility, leading to improved overall capacitance (Xu et al., 2008).

AC from biomass sources like coconut shells and lignocellulosic materials, provides sustainable options for large-scale production. Current studies in hierarchical pore design and composite integration focus on enhancing these biomass derived AC performance for future supercapacitors.

1.9 Electrochemical Evaluation Techniques

1.9.1 Two Electrodes Vs. Three Electrode Systems

Table 1: *Two Electrodes vs. Three Electrode Systems*

Feature	**Two-Electrode System**	**Three-Electrode System**
Purpose	Examines the performance of the entire device, including actual real-world consequences (Conway, 2013).	Concentrates on the detailed examination of a single electrode material (Zhang & Zhao, 2009).
Setup	Two equivalent electrodes with separator and electrolyte placed in between (Simon & Gogotsi, 2008).	One working electrode, one reference electrode, and a counter electrode (Brett & Brett, 1993).
Current Flow	Current passes between the two working electrodes.	Current passes between the working and counter

		electrodes; reference electrode carries almost no current.
Measured Performance	Reflects the combined behavior of both electrodes and all cell components.	Isolates the behavior of the working electrode only.
Realism	Simulates how an actual device would behave in practice.	Represents ideal performance without considering real-world resistances.
Capacitance Values	Generally lower, more realistic values.	Typically higher, due to minimized losses.
Common Use	Used in device prototyping, commercialization, and testing of full cell.	Used in preliminary material research and optimization of electrodes.
Limitation	Hard to determine individual electrode contribution.	The results might exaggerate real device performance.

1.9.2 Performance Metrics of Electric Double-Layer Capacitors (EDLCs)

Table 2: *Performance metrics of EDLCs*

Parameter	Typical Range	Remarks	Source
Specific Capacitance	100–200 F/g	Based on activated carbon electrodes and common electrolytes.	(Conway, 2013)
Energy Density	5–10 Wh/kg	Practical range for commercial EDLCs.	(Zhang & Zhao, 2009)
Power Density	1,000–10,000 W/kg	Very high due to rapid charge/discharge capability.	(Simon & Gogotsi, 2008)
Equivalent Series Resistance (ESR)	0.01–0.5 Ω	Lower ESR improves efficiency and power delivery.	(Brett & Brett, 1993)

1.10 Jacaranda Seed Pods: An Underutilized Biomass for AC

Jacaranda mimosifolia, semi-deciduous trees native to South America. They are also spread wide across different tropical and subtropical regions, inhibiting blue color flowers with brown woody seed pods. The disc-like, hard, dry, flattened seed pods are discarded as a biowaste. These pods function as a protective layer for seed storage, aiding in seed dispersal. Lignocellulosic biomasses like Jacaranda seed pods primarily contain cellulose, hemicellulose, and lignin suitable for the preparation of activated

carbon (AC). Under elemental analysis, these pods have high carbon content with moderate volatile substances and some low ash. Besides, the presence of inherent minerals like potassium, calcium, and magnesium, can enhance the pore development within the activated carbon during pyrolysis (Treviño-Cordero et al., 2013).

There are different studies conducted relating to the potential of Jacaranda seed pod-derived activated carbon in environmental remediation. They showed good adsorption performance in the removal of heavy metals (lead and cadmium) and dye molecules (methylene blue) from aqueous solutions (Treviño-Cordero et al., 2013). These fields utilize the pod's high specific area, porous structure, and oxygen-inhibiting surface functional groups. Chemical activation processes like acid activation (using H_3PO_4) and base activation (using KOH), significantly develop the pore formation, manifesting the material competitiveness with other biowastes. Moreover, AC from Jacaranda seed pods shows promising results in the removal of ketoprofen (a pharmaceutical contaminant) from water (Georgin et al., 2021). Thus, the high porosity and surface functionality facilitate the efficient and economic adsorption material to remove such organic pollutants.

While Jacaranda seed pods exhibit promising features, they remain untapped for energy storage applications, in particular the activated carbon electrode development. Despite activated carbon from different biowastes being investigated for supercapacitor applications, Jacaranda pod-derived AC electrochemical properties remain undisclosed. Surface area functionalization, mesopores and micropores tuning, and electrical conductivity improvement come under the key areas of focus (John Chmiola et al., 2006). This gap could open an alternative pathway for the utilization of such underutilized abundant biomass into a sustainable value-added product for energy storage systems.

Table 3: *Summary of bio-mass derived AC for EDLC application using different electrolytes*

Precursor	Temp (°C)	Activating Agent	BET (m^2/g)	Current Density (A/g)	Capacitance (F/g)	References
Orange Peel	800	KOH	2004	0.5	306.6	(Shen et al., 2019)
Bamboo	900	KOH	2221.1	0.5	293	(Zhang et al., 2018)
Pine Saw Dust	900	KOH	2330.89	0.5	175.6	(Quan et al., 2020)
Pinus pinaster Needle	800	H_3PO_4	281.4	0.25	68	(Yumak, 2021)
Walnut Shell	800	H_3PO_4	1956	0.2	46	(Pavlenko et al., 2018)
Baobab Fruit Shell	800	H_3PO_4	911.7	1	355.8	(Mohammed et al., 2019)
Rice Husk	850	KOH	2696	0.1	147	(Liu et al., 2016)
Pinus pinaster Cone	800	H_3PO_4	868.4	0.25	106	(Yumak, 2021)

1.11 Objectives

General Objective

- To prepare activated carbon form Jacaranda Seed pods as anode material and evaluate its electrochemical properties.

Specific Objectives

- Preparation of activated carbon from Jacaranda Seed pods using H_3PO_4 as activating agent.
- Characterization of Activated Carbon.
- Study of electrochemical properties of Activated Carbon as an anode material.

1.12 Organization of Dissertation

Chapter 1. This chapter manifests the background and motivation for the project and its research objectives.

Chapter 2. This chapter presents the literature review on the activation techniques, activated carbon surface characteristics, fundamentals and working principle of supercapacitors, the role of electrolytes and electrodes in supercapacitors, electrochemical evaluation techniques, and the potential of Activated Carbon from the Jacaranda Seed Pods.

Chapter 3. This chapter details the materials used and the methodology performed for material synthesis and characterization.

Chapter 4. This chapter discusses the results of physicochemical characterization and analysis of the electrochemical experiments.

Chapter 5. This chapter relies on the result summary, conclusion, and future scope of the study.

CHAPTER 2: LITERATURE REVIEW

Traditionally ACs are derived from coal and petroleum-based precursors, which overall increases the carbon footprint as well as production cost. Therefore, the researchers are inclined towards biomass-based alternatives (Abuelnoor et al., 2021). The surface morphology, hierarchical pore structure, and surface functionalities have been extensively studied for these biomasses as they offer a renewable, cost-effective, and sustainable carbon source. Further they are compatible with different structural and surface modifications (Du et al., 2020).

Different waste biomass precursors such as coconut shells, sugarcane bagasse, peanut shells, sawdust, banana peels, rice husks, etc. have been investigated due to their rich carbon content, meso-micro pores formation upon physical (using gases like steam or CO_2) or chemical activation (using agents like KOH, $ZnCl_2$, H_3PO_4, etc.) (Gayathiri et al., 2022).

Adsorption and electrochemical properties of AC-derived biomasses have been widely affected by the volume of micropores and mesopores present. Further, doping (using nitrogen, and sulfur) through intrinsic biomass content or post-treatment can further augment the electronic conductivity, specific capacitance, and wettability of the prepared material (Balou et al., 2020).

Different organic materials come from plants like seeds, leaves, bark, shells, etc. These organic materials include hemicellulose, cellulose, lignin, proteins, lipids, sugars, carbohydrates, sugars, water, ash, and other significant compounds. The trending energy crisis and global warming have made everyone diverge from fossil fuel reliance and look into these plant-based biomasses as a clean energy alternative because of their renewability, abundance, and eco-friendliness (Srirangan et al., 2012). 42-47 % Carbon (C), 40-44 % Oxygen (O), and 6 % Hydrogen (H) are the major elements of plant biomass. Other components (macronutrients) for biomass production are: nitrogen(N), potassium(K), phosphorous(P), calcium (Ca), sulfur (S), and magnesium (Mg). Furthermore, other trace elements like sodium (Na), iron (Fe), copper (Cu), chlorine (Cl), etc. are also present in small amounts (Bhatla & Lal, 2023; Sinha & Tandon, 2020). However, cellulose, hemicellulose, and lignin are the major structural components of plant biomass. Lignin influences the carbon yield, structural stability, and presence of functional groups inside the activated carbon derived from biomass. Cellulose and

hemicellulose contribute to the pore formation enhancing the surface area of AC (Boundzanga et al., 2022; Cagnon et al., 2009).

Different lignocellulosic biomasses-derived activated carbon show disparate electrochemical behavior with distinct activating agents, electrolytes, temperature, and concentration variations. Tea waste-derived activated carbon on activation with KOH at 700 °C had a surface area of 1610 m^2 g^{-1} and a specific capacitance of 332 F g^{-1} at 1 A g^{-1} in 6M KOH (Khan et al., 2020). *Elaeocarpus tectorius* shell under chemical activation with phosphoric acid at 900 °C showed a specific capacitance of 385 F g^{-1} at 1 A g^{-1} with a surface area of 860 m^2 g^{-1} in 1 M H_2SO_4 (Hou et al., 2015). Betel nut at 800 °C under nitric acid activation showed specific capacitance of 423 F g^{-1} at 0.5 A g^{-1} in 6 M KOH (Fang et al., 2019). Similarly, the *Tamarindus indica* fruit shell showed a specific capacitance of 285 F g^{-1} at 1 A g^{-1} in 1 M KOH under phosphoric acid activation. Also, the specific surface area was 847 m^2 g^{-1} (Sivachidambaram et al., 2019). Furthermore, Kapok fibers under potassium hydroxide activation at 850 °C showed higher surface area 3010 m^2 g^{-1} with specific capacitance of 144 A g^{-1} at 0.2 A g^{-1} in 1 M $TEABF_4$/ PC (Zou et al., 2019).

Extensive research has been conducted on utilizing lignocellulosic biomasses as electrodes in supercapacitor applications. However, Jacaranda Seed pods as a carbon precursor and its activated carbon utilization for electrodes in supercapacitors remain unexplored to date. The study of carbonization behavior, micro-mesopores formation, and electrochemical performance of Jacaranda Seed Pods explains the notable gap in this field. Therefore, exploration of this under-utilized biomass could lead to the discovery of sustainable, eco-friendly, and highly efficient electrodes for supercapacitor applications.

CHAPTER 3: EXPERIMENTAL SECTION

3.1 Materials

3.1.1 Laboratory Requirements

1. Apparatus: Beaker, Measuring Cylinders, Centrifuge Tubes, Viles, Nickel Foam, Micropipette, and Agate Mortar & pestle sets were used.
2. Instruments: Mixture Grinder, Ultrasonic Cleaner, Tube Furnace (Kejia Furnace), Centrifuge Machine (BIOBASE), Oven, and Electrochemical Workstation (CorrTest) were used.
3. Chemicals: Orthophosphoric Acid [H_3PO_4 (85% pure, SRL)], Ethanol (99 % pure), Hydro Chloric Acid [HCl (35% pure)], Potassium Hydroxide [KOH (85% pure, Fisher Scientific)], Iso Propyl Alcohol [99% pure, CDH], and Polyvinylidene fluoride were used.

The chemicals were used as-obtained without any further purification.

3.2 Research Methodology

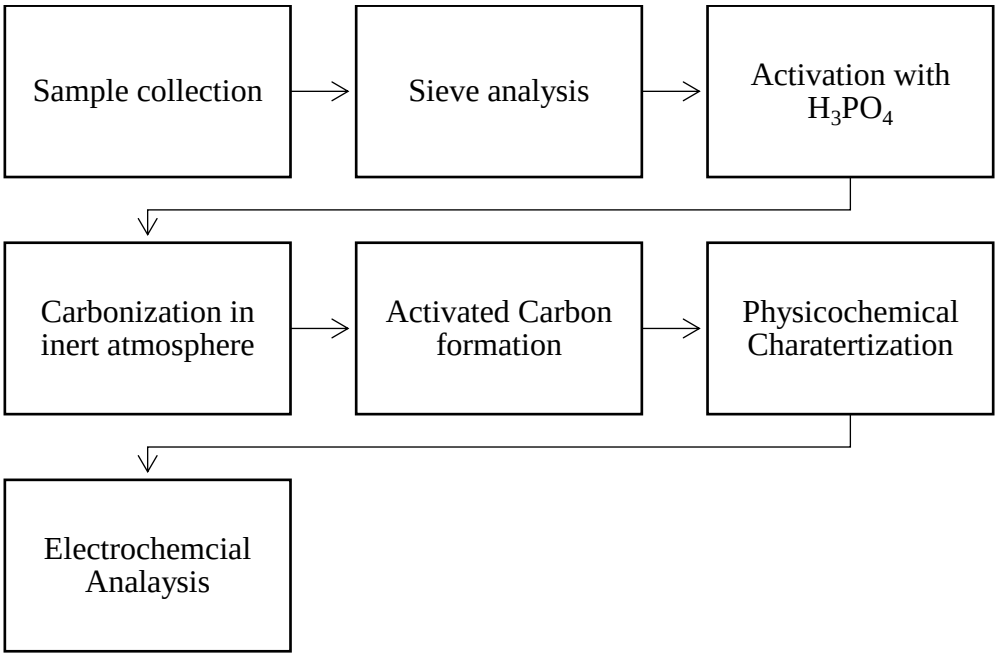

Figure 6 *Schematic Diagram of preparation of Activated Carbon, Physicochemical Characterization and Electrochemical Analysis*

3.3 Activated Carbon Preparation

3.3.1 Sample Preparation

Dried Jacaranda seed pods were collected from Pulchowk Campus, Lalitpur, Nepal. The collected pods were washed thoroughly with distilled water, and then oven-dried at 60 °C for 24 h. The dried seed pods were then grinded into fine powder. The powder was passed under a sieve of 106 µm. The sieved powder was again dried at 60 °C for 24 h.

Figure 7 *Jacaranda Seed Pods and Powder*

3.3.2 Phosphoric Acid Activation

Then, 10 g of Jacaranda fine powder was mixed with 30 g of orthophosphoric acid (85% pure) in impregnation ratio of 1:3, which was mixed thoroughly and left for a day to form a homogenous paste. The obtained paste was then further oven-dried at 60 °C for 24 h.

Figure 8 *Chemical Activation using Phosphoric Acid*

3.3.2 Carbonization of JSP with Acid Impregnation

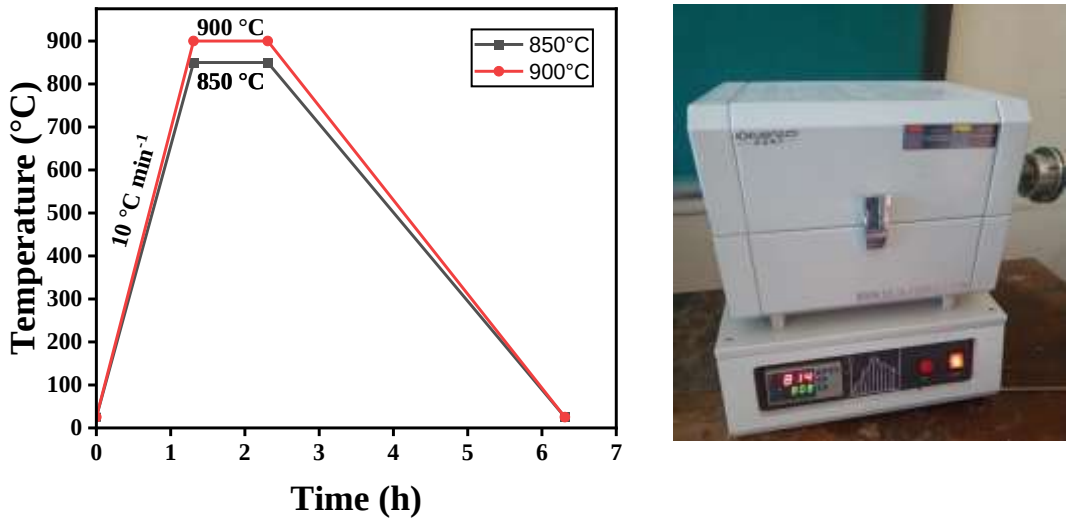

Figure 9 *Carbonization in Tube Furnace with Nitrogen Atmosphere*

Thus, prepared paste was subjected to carbonization in an inert atmosphere of N_2 gas at 850 °C and 900 °C for 1 h in a tube furnace with ramping temperature of 10 °C min^{-1}. The carbonized mass was washed with distilled water repeatedly and collected after centrifugation. Furthermore, the sample was oven-dried for 12 h. The final sample obtained was then named Activated Carbon from Jacaranda Seed Pods Prepared at 850 °C (ACJSP-850) and 900 °C (ACJSP-900) respectively.

3.4 Analytical Methods

3.4.1 Fourier Transform - Infrared Spectroscopy (FTIR)

The molecular bonds absorb specific frequencies of infrared light, and vibration of molecular bonds are caused at those certain specific frequencies. This is the core principle of FTIR spectroscopy. Under the broad spectrum of IR radiation, the sample absorbs light at characteristics frequencies to its molecular structure. The resulting signal is transformed mathematically using Fourier Transformation forming a spectrum. Thus, the absorption/transmittance peaks correspond to different functional groups in the specimen (Dutta, 2017).

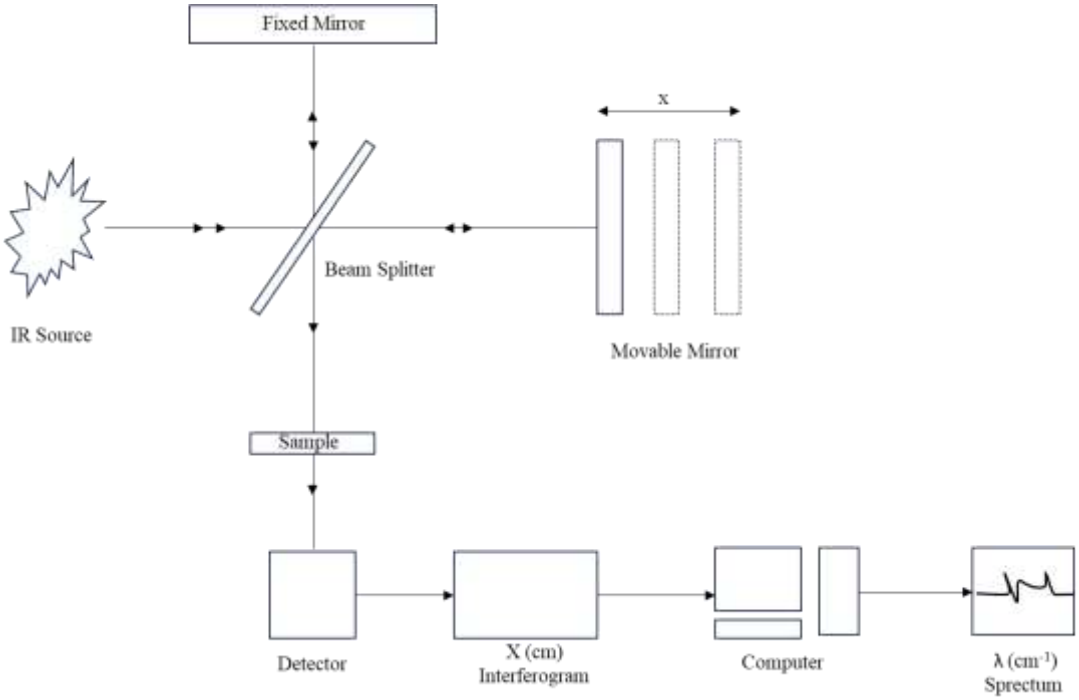

Figure 10 *Working principle of FTIR*

Fourier Transform Infrared (FTIR; PerkinElmer Spectrum IR version 10.6.2, Amrit Campus, Thamel, Kathmandu) was used to determine the different functional group of pristine sample vs prepared activated carbon within the IR range of 500-4000 cm^{-1}.

3.4.2 X-Ray Diffraction (XRD)

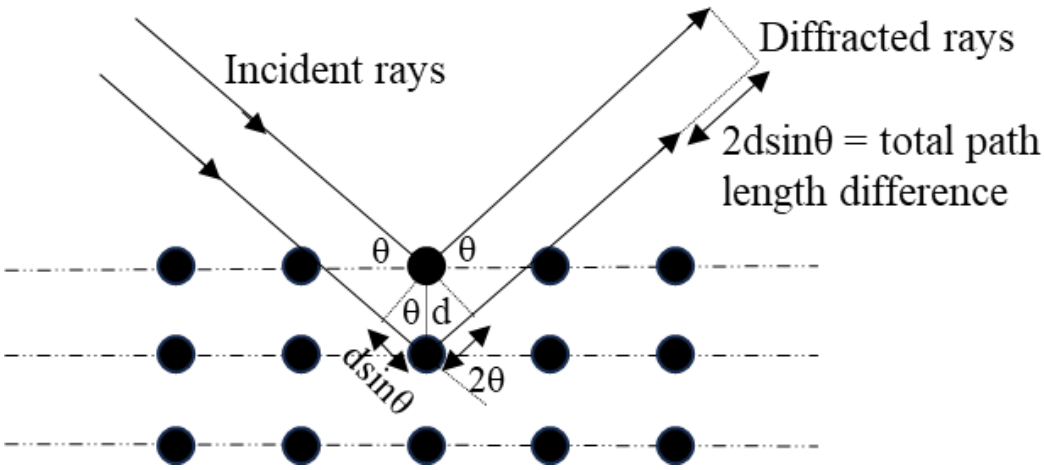

Figure 11 *Visual Representation of Bragg's Law*

X-ray diffraction (XRD) uses Bragg's law to determine the crystalline structure of solid materials. The X-rays strike the crystal lattice and form constructive interference at

certain specific angles to satisfy Bragg's condition. Mathematically, Bragg's Law is represented by (Epp, 2016):

$n\lambda = 2d \sin\theta$ ……. (2)

Here,

n - order of reflection,

λ - wavelength of the X-ray,

d - interplanar spacing between the atomic planes, and

θ - angle of incidence.

XRD further helps in determining the Full Width at Hob Maxima (FWHM), Peak Width, Peak Intensity, Angle of incidence (θ), and Peak Shift (Bakshi et al., 2018).

Similarly, the crystallite size from XRD can be determined using the Debye-Scherrer equation (Holzwarth & Gibson, 2011):

$D = (K\lambda) / (\beta \cos\theta)$ ……. (3)

Here,

K - shape factor (nearly 0.9)

λ - means X-ray wavelength,

β - Full Width at Hob Maxima,

and θ - Bragg's angle.

The D2-Phraser X-ray Diffractometer analysis, from Nepal Academy of Science and Technology (NAST), was performed to determine the characteristics of prepared ACJSP-850 and ACJSP-900.

3.4.3 Field Emission Scanning Electron Microscope and Energy Dispersive Spectroscopy (FESEM and EDX)

The Field Emission Scanning Electron Microscope (FESEM) utilizes a focused beam of high-energy electrons emitted from a field emission gun to scan the sample surface to create a high-resolution 2D- image. When interacting with the atoms of the sample, the main electron splits into secondary electrons (SE), and backscattered electrons (BE) and produces characteristics of X-rays. The secondary electrons are primarily utilized to create a high-resolution image, giving information on surface morphology and

topography at the nano-level. The electron beam produced by FESEM is sharper and the energy utilized is lower compared to SEM (Abd Mutalib et al., 2017).

Further, the incorporation of Energy Dispersive Spectroscopy (EDS) helps to identify as well as quantify the elemental composition of the sample. The high-energy electrons strike the atom causing the ejection of inner-shell electrons from atoms, filling the vacancy with higher-energy electrons and emitting X-rays of characteristics of each element. These emitted X-rays are further categorized and analyzed to determine the elemental composition and relative concentrations (Nandee et al., 2024).

The surface morphology of as-synthesized AC was carried out by Field Emission Scanning Electron Microscope (FESEM; JBNU CURF EM Lab) at an accelerating potential of 2.0 kV integrated with an Energy Dispersive X-ray (EDX) spectroscope to identify the elemental composition.

3.5 Electrochemical Measurement

3.5.1 Electrode Preparation

Figure 12 *Electrochemical Workstation and Activated Carbon Electrode*

Figure 12 demonstrates the overall electrochemical testing of activated carbon using electrochemical workstation in 3 electrode system. Firstly, nickel foam of 1 cm^2 was sonicated in 1 M HCl followed by water and ethanol to remove any impurities and dried at 80 °C for 8 h. 4 mg of AC, 0.5 mg of PVDF, and 0.5 mg of carbon black with a ratio of 8:1:1 was ground, formed into a slurry using isopropyl alcohol, and drop-casted into the nickel foam of 1 cm^2 to form a working electrode. Similarly, platinum wire and

Ag/AgCl were used as counter electrode and reference electrode, respectively, in the three-electrode system. Furthermore, 6 M KOH solution was used as an electrolyte.

3.5.2 Cyclic Voltammetry (CV)

Cyclic Voltammetry (CV) provides insights to the electrochemical behavior of electrode materials. In CV, a current on working electrode is measured against linearly varying voltage applied in a cyclic manner. This further reveals the nature of the electrode material, and its oxidation and reduction peaks.

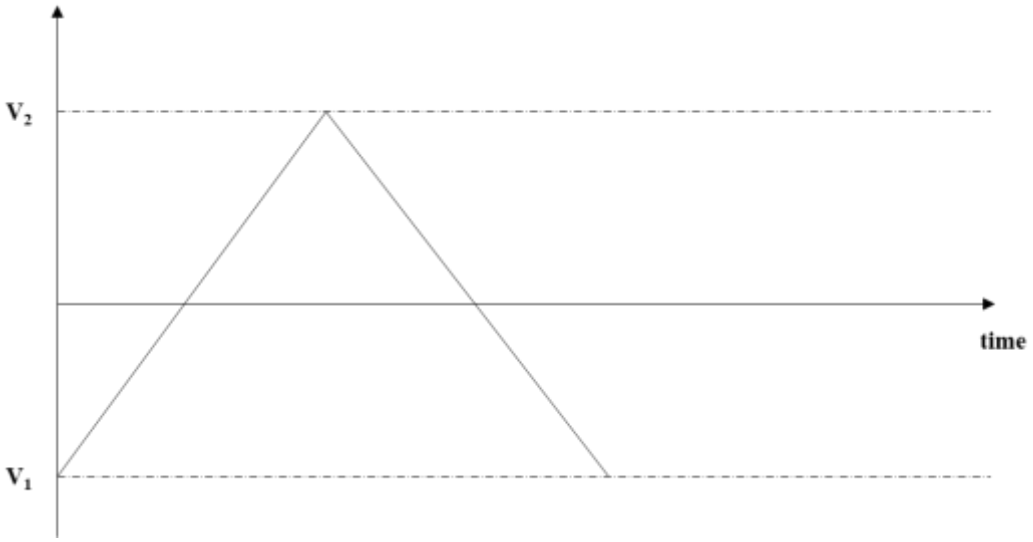

Figure 13 *Potential is swept between V_1 and V_2 for CV measurement*

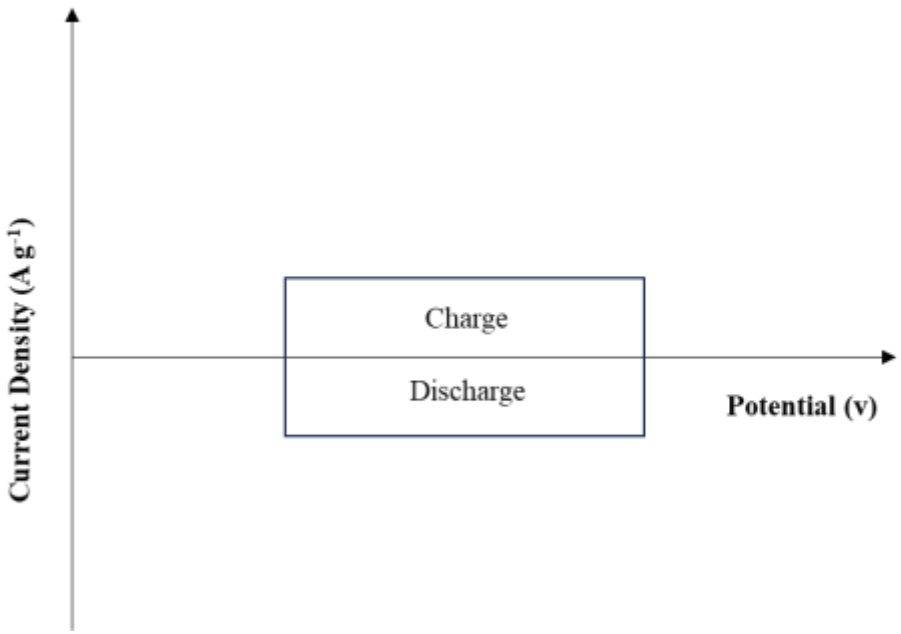

Figure 14 *CV for an EDLC without faradic reaction*

This shape further gives insights into the reversibility, kinetics, capacitance behavior and charge storage mechanism of the electrode. The specific capacitance (C_s) given by (Abd Mutalib et al., 2017):

$$C_s = \frac{\int I(V)dV}{2m\Delta V\nu} \ldots\ldots\ldots\ldots (4)$$

$\int I(V)\, dV$ = area under the CV plot (A·V)

m = mass of the active material (g)

ΔV = voltage window (V)

ν = scan rate (mV/s)

CV plot further helps to determine charge storage mechanism of from b-value analysis and Dunn's method.

b-value analysis indicates the charge storage mechanism (ideal capacitive or diffusion controlled) based on the plot between the scan rate (ν) and peak value current (i) (Girard et al., 2015). Mathematically,

$$i = a \cdot \nu^b \ldots\ldots\ldots\ldots\ldots (5)$$

Taking logarithm on both side:

$$\log(i) = \log(a) + b \cdot \log(\nu) \ldots\ldots\ldots (6)$$

i - peak current (A)

v – scan rate (mV/s)

a – constant

b – slope

Dunn's method is an approach to separate the total current response in CV into capacitive and diffusion-controlled contributions (Tiwari et al., 2019). The Dunn's equation is given by:

$$i(V) = k_1 \cdot \nu + k_2 \cdot \nu^{1/2} \ldots\ldots\ldots (7)$$

$$\frac{i(V)}{\nu 1/2} = k_1 \cdot \nu^{1/2} + k_2 \ldots\ldots\ldots (8)$$

From eq (7)

i(V)- current at a specific potential V,

$k_1\nu$ – capacitive behavior, $k_2 \cdot \nu^{1/2}$ - diffusion-controlled behavior

3.6.2 Galvanostatic Charge Discharge (GCD)

The GCD helps to determine the nature of supercapacitor i.e. pseudo capacitors or electric double-layer capacitors (EDLCs). The GCD measures the voltage with respect the applied constant charging and discharging current over time.

The GCD test provides information into the Columbic efficiency, internal resistance (IR drop), and rate capability. The specific capacitance (C_s) is given by (Mukhiya et al., 2019) :

$$C = \frac{I * t_d}{g * V} \quad \ldots\ldots\ldots\ldots\ldots (9)$$

From equation (9),

C is the specific capacitance (F g^{-1}), t_d is the discharge time (s), V is the voltage difference in discharge (V), I is the constant discharge current (A), and m is the active electrode material (g).

Similarly, the columbic efficiency is given by (Laheäär et al., 2015):

$$\eta\ (\%) = \frac{t_{charge}}{t_{discharge}} \times 100 \quad \ldots\ldots\ldots (10)$$

From equation (10),

t_{charge} – charging time,

$t_{discharge}$ – discharging time

The GCD curve was obtained at different current densities. Further, charging and discharging time was determined.

3.6.2 Electrochemical Impedance Spectroscopy (EIS)

Electrochemical Impedance Spectroscopy is the curve obtained when small AC voltage is applied over a range of frequencies (0.01 Hz to 100000 Hz). This curve helps to analyze the capacitive behavior, electrical resistance and the equivalent circuit of the electrochemical systems.

The resisting behavior when AC current is pass through it gives the overall impedance of the material. Impedance can further be divided into real part (resistance) and imaginary part (reactance). The following equations is used to determine Impedance (Z) (Magar et al., 2021).

$$Z(\omega)=Z' + jZ''\ldots\ldots (11)$$

From eq (11)

ω (2πf) – angular frequency

Z' – resistance

Z'' - reactance

Hence, further equivalent series resistance (ESR), capacitance (C), and equivalent circuit of the electrochemical devices can be constructed using EIS curve (Magar et al., 2021).

CHAPTER 4: RESULTS AND DISCUSSION

4.1 Physicochemical Characterization

4.1.1 Effect of Carbonization Temperature on Activated Carbon Yield from JSP Precursor

Table 4: *Effect of Carbonization Temperature on Activated Carbon Yield from JSP Precursor*

Precursor JSP (g)	Carbonization Temperature	Retained Activated Carbon (g)	Percentage Yield (AC)
10 g	850 °C	1.2 g	12 %
10 g	900 °C	1.47 g	14.7 %

From Table 4, initially 10 g of Jacaranda Seed Powder (JSP) was activated with phosphoric acid at 1:3 Impregnation Ratio. 1.2 g of AC was obtained after carbonization at 850 °C, and 1.47 g of AC was formed at 900 °C.

4.1.2 Fourier-transform infrared (FTIR) analysis

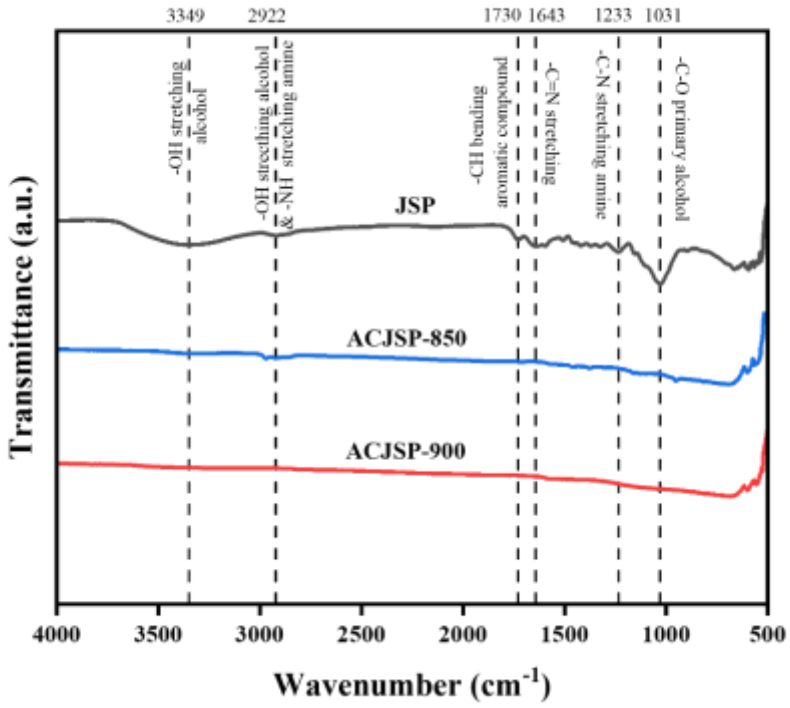

Figure 15 *Fourier transform infrared (FTIR) analysis spectra of pristine Jacaranda Seed Powder and Carbonized Jacaranda Seed Powder*

Table 5: *FTIR Data Interpretation of Pristine Jacaranda Powder Sample and Carbonized Jacaranda Powder Sample*

Wavenumber (cm^{-1})	Functional Group	JSP	ACJSP-850	ACJSP-900
3349	-OH Stretching alcohol	Present	Absent	Absent
2922	-OH Stretching alcohol & -NH stretching amine	Present	Absent	Absent
1730	-CH bending aromatic compound	Present	Absent	Absent
1643	-C=N Stretching	Present	Absent	Absent
1233	-C-N stretching amine	Present	Absent	Absent
1031	-C-O primary alcohol	Present	Absent	Absent

Figure 15 Jacaranda Seed Powder (JSP) shows the formation of single bond region (2500-4000 cm^{-1}). There is presence of the -OH Stretching alcohol group at 3349 cm^{-1}. Also, the peak at 2922 cm^{-1} shows the presence of -OH Stretching alcohol and -NH stretching amine group. No peak at triple bond region (2000-2500 cm^{-1}) is seen in the pristine JSP. In the double bond region (1500-2000 cm^{-1}), the peak at 1730 cm^{-1} corresponds the presence of -CH bending aromatic compound, and the peak at 1643 cm^{-1} signifies the presence of -C=N Stretching group. At 1233 cm^{-1} -C-N stretching amine group is present and at 1031 cm^{-1} -C-O primary alcohol group is present (Berthomieu & Hienerwadel, 2009).

The carbonized Jacaranda Seed Powder (ACJSP-850 & ACJSP-900) shows the absence of all those compounds, which concludes that no organic impurities are present in the carbonized sample. This further verifies the proper carbonization of the pristine sample with graphitic carbon framework. Further there is no redox reaction happening due to the absence of different functional groups. Additionally, it also hints towards the electric double-layer capacitor behavior.

4.1.2 FESEM and EDX analysis

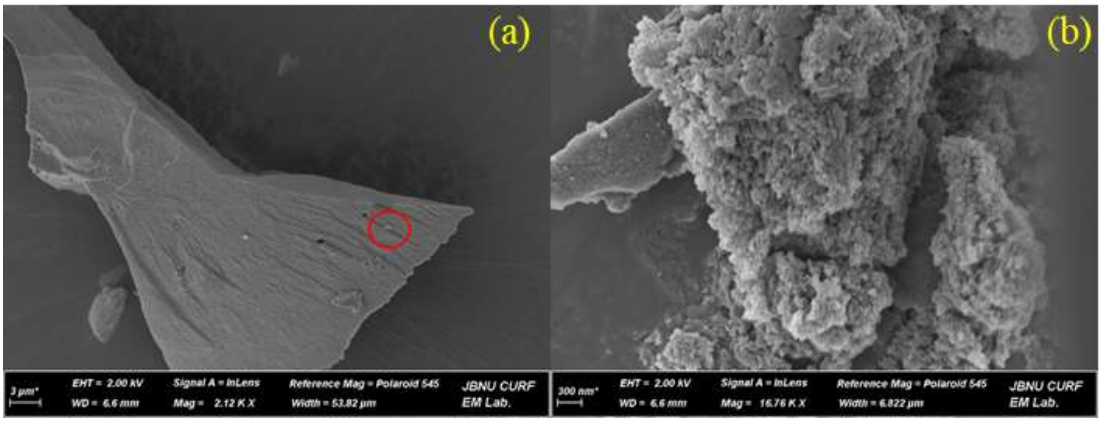

Figure 16 *SEM image of Prepared ACJSP-850*

The structural switch in the surface morphology of activated carbon (ACJSP-850) was confirmed by FESEM. Figure 16 (a) and Figure 16 (b) confirmed the carbon activated using ortho-phosphoric acid under 850 °C for 1 h under N_2 atmosphere exhibited a sponge-like porous structure within a magnification level of 3 µm and 300 nm. This verified the morphological evolution with formation of mesopores and micropores for better ion diffusion.

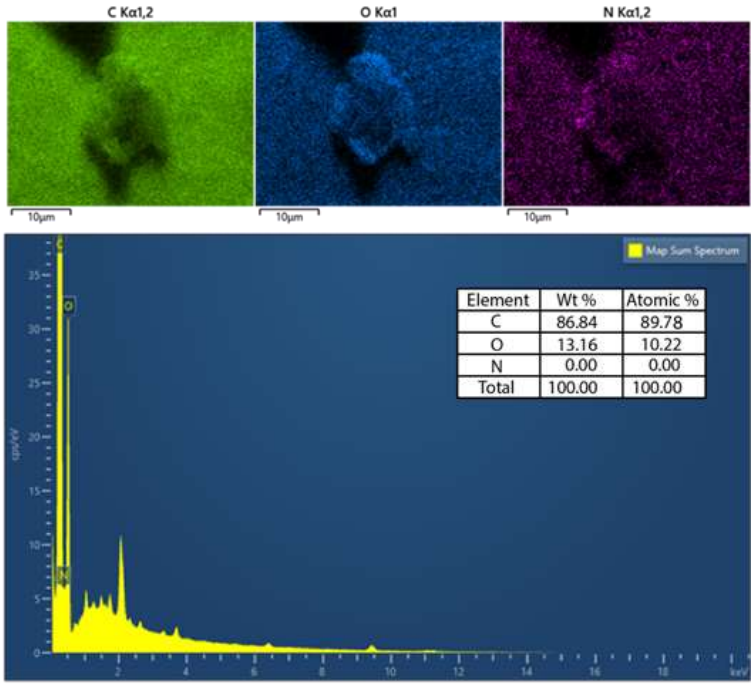

Figure 17 *EDX analysis and Mapping of Prepared ACJSP-850*

Furthermore, elemental mapping of the prepared ACJSP-850 showed the presence of three major elements i.e. carbon, oxygen, and nitrogen as shown in Figure 17. In addition, EDX spectra also clarified the presence of carbon (88.78%), oxygen (10.22%)

by atomic weight, and no detectable nitrogen gas in the synthesized ACJSP-850. The low oxygen and high carbon content justified the ion conductivity with EDLC behavior omits any pseudocapacitive nature.

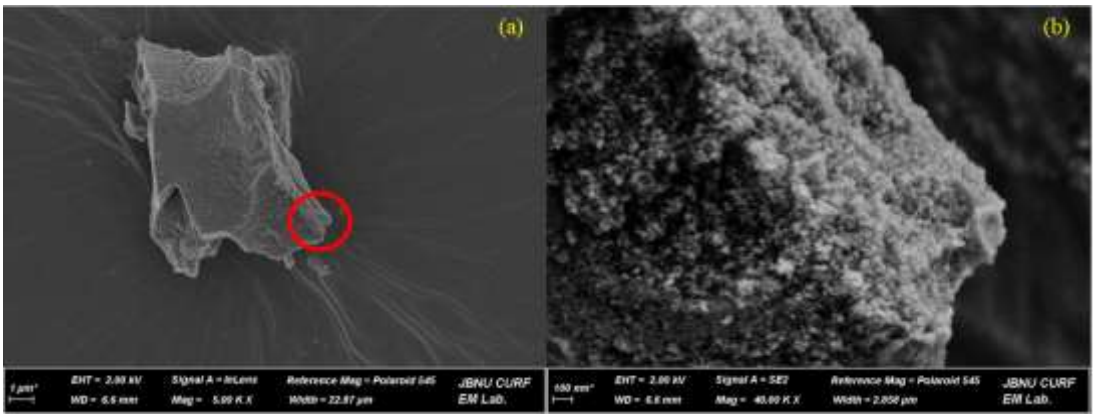

Figure 18 *SEM image of Prepared ACJSP-900*

Similarly, the surface morphology of activated carbon (ACJSP-900) was observed through FESEM. Figure 18 (a) and Figure 18 (b) confirmed the formation of highly porous activated carbon and the presence of mesopores and micropores at a magnification level of 100 nm. The high surface roughness reveals the presence of more active mass sites for ion adsorption supporting partial graphitization and ion conductivity through large pore channels.

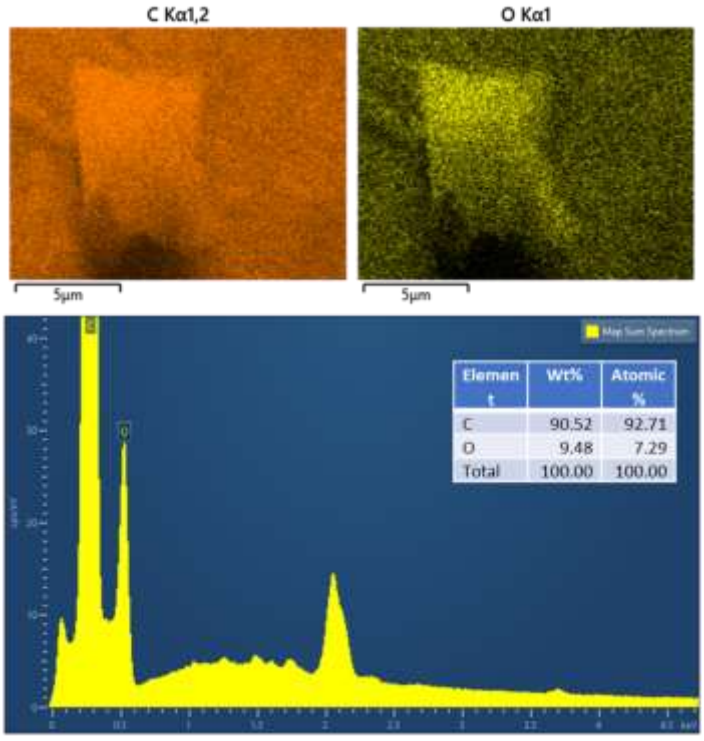

Figure 19 *EDX analysis and Mapping of Prepared ACJSP-900*

The EDX analysis of the prepared ACJSP-900 showed the presence of carbon and oxygen as shown in Figure 19. In addition, it is quite evident that the formed material is pure activated carbon due to the presence of carbon (92.71%) and oxygen (7.29%) by atomic weight at 900 °C. This shows the EDLC type behavior of the electrode material omitting any faradic reaction.

4.1.2 X-Ray Diffraction (XRD) analysis

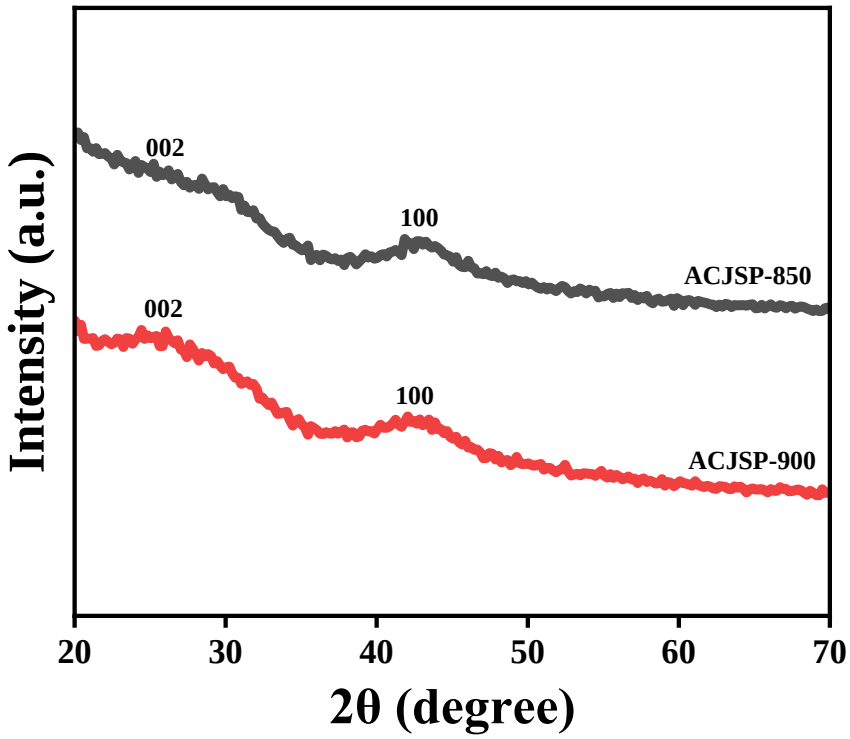

Figure 20 *XRD analysis of activated carbon at different temperatures*

Table 6: *Lattice planes, d-Spacing and Crystallite Size of ACJSP*

Peaks	Planes	d-spacing Braggs Law (nm)	Crystallite Size Debye–Scherrer equation (nm)
26 °	002	0.343	1.04
43 °	100	0.21	-

Figure 20 and Table 6 shows that both the activated carbon prepared at 850 °C and 900 °C have significant peaks at 26° and at 43°. This highlights the graphitic-like stacking of carbon layers. The broad peak at the 002 planes reflects the amorphous nature of the

activated carbon with increased d-spacing (0.343 nm) i.e. turbostratic carbon with disordered structures. Further, the peak at 43° has d-spacings of 0.21 nm corresponding to 100 planes indicating some degree of sp^2 hybridization within the carbon matrix. This suggests the presence of more continuous and well-ordered C=C bonding networks revealing graphitic domains. This further enhances the conductivity of prepared activated carbon due to the higher degree of graphitization. The average size of individual crystallite domains of activated carbon as per XRD interpretation is 1.04 nm.

4.2 Electrochemical Characterization

4.2.1 Cyclic voltammetry (CV)

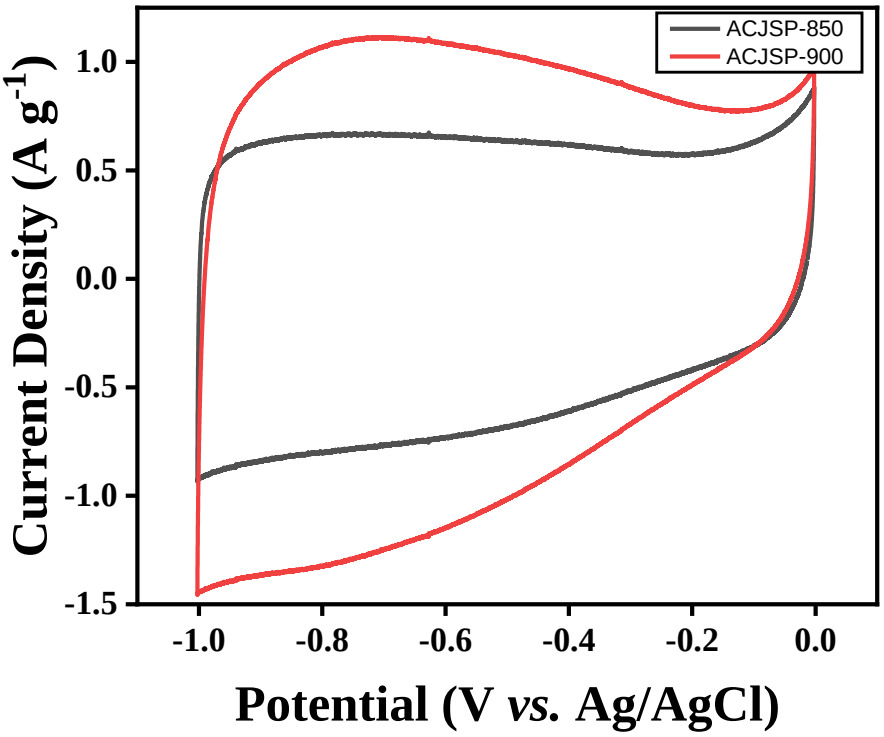

Figure 21 *CV curve of ACJSP-850 and ACJSP-900 at 5 mV s^{-1}*

Figure 21 represents the comparative Cyclic Voltammetry (CV) curves of AC from Jacaranda Seed Pods at a scan rate of 5 mV s^{-1}. At this scan rate the AC prepared at higher temperature i.e. 900 °C shows a broader quasi rectangular curve compared to the AC prepared at 850 °C. This revealed the formation of electric double layer capacitor (EDLC). Further it also provides insights on the mechanism of charge storage happening between the electrode-electrolyte interface. Also compared to ACJSP-850, the ACJSP-900 has higher surface area.

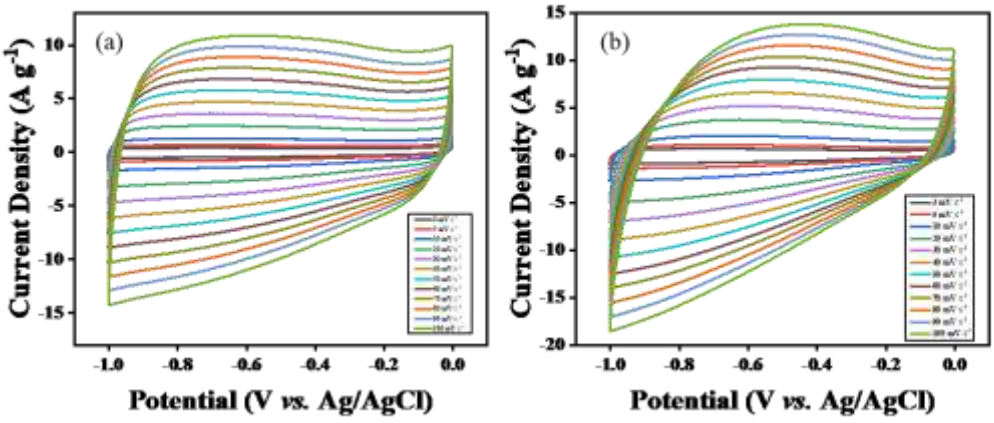

Figure 22 *CV curve of (a) ACJSP-850 & (b) ACJSP-900 at different scan rates*

The Cyclic Voltammetry (CV) curves of AC Jacaranda Seed Pods electrode revealed a symmetrical and quasi-rectangular nature showing the potential of supercapacitors, with no obvious redox peaks at scan rates 3 mV s^{-1}, 5 mV s^{-1}, 10 mV s^{-1}, 20 mV s^{-1}, 30 mV s^{-1}, 40 mV s^{-1}, 50 mV s^{-1}, 60 mV s^{-1}, 70 mV s^{-1} , 80 mV s^{-1} , 90 mV s^{-1} and 100 mV s^{-1} as shown in Figure 22. This suggested that double electric layers primarily generated the capacitance of supercapacitors during the charging-discharging process. Hence, the charge storage in the activated carbon is of EDLC form. In the CV curve, Electric Double-Layer Capacitors (EDLCs) display unique traits that indicate how they store energy. Energy storage in EDLCs occurs by electric charge buildup at the electrode-electrolyte interface, rather than faradic reactions. Thus, the area inside the curve represents electrostatic charge accumulation due to the formation of a Helmholtz layer and a diffuse layer at the electrode-electrolyte interface. This also clarifies that the greater the area of the curve, the higher the specific capacitance (Mukhiya et al., 2021).

While the area of the curve on ACJSP-900 is higher than that of ACJSP-850, the CV curve is more distorted at higher scan rates. This shows the presence of greater resistance in the ACJSP-900 between the electrode-electrolyte interface thus resulting in the slower ion diffusion rate. However, curve distortion and resistance of ACJSP-850 is lower at higher scan rate, but the charge storage capacity of ACJSP-850 is slightly lower due to its lower surface area.

Factors Affecting CV curve in Electrochemical Test:

The redox species concentration, electrode material, and surface area, and electrolyte composition are all important factors in determining the shape of the cyclic voltammetry (CV) curve. Increased levels of redox-active substances enhance the

current response, as a greater number of electrons are exchanged during the electrochemical process, resulting in higher peak currents. The CV curve is heavily influenced by both the electrode material and its surface area, with conductive or catalytically active materials improving electron transfer kinetics and larger surface areas or rough electrode surfaces increasing reaction sites, thereby increasing current. Finally, the ion conductivity in the solution is affected by the electrolyte composition. An electrolyte that is highly conductive helps to facilitate the movement of ions effectively, leading to decreased resistance and yielding more uniform cyclic voltammetry curves. On the other hand, electrolytes with low conductivity can result in higher solution resistance, causing distorted or shifted peaks and influencing the overall response (Ward et al., 2012).

b-value Analysis:

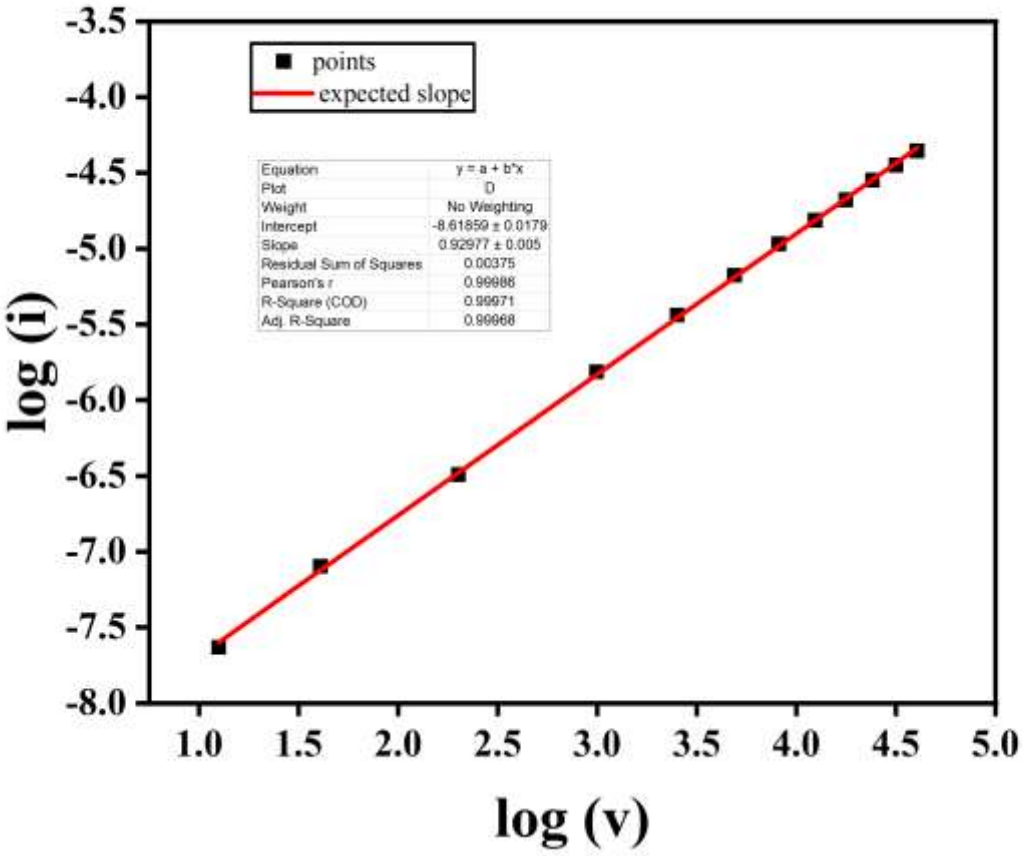

Figure 23 *b-value analysis of ACJSP-850*

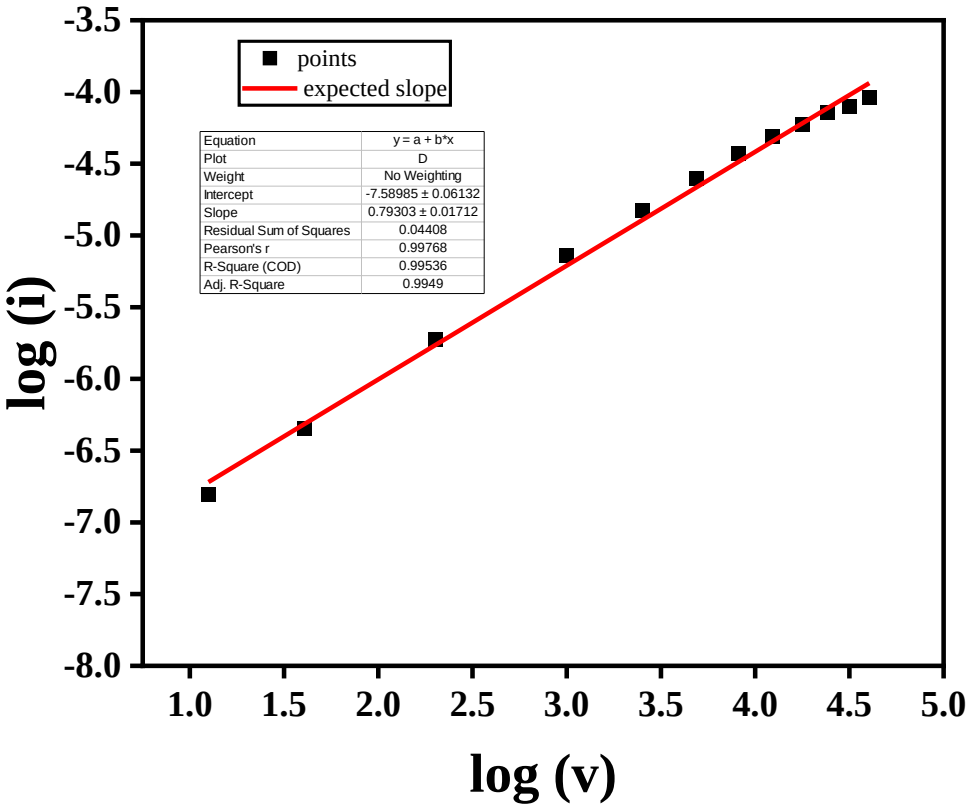

Figure 24 *b-value analysis of ACJSP-900*

From Figure 23 and Figure 24, the b-value of ACJSP-850 and ACJSP-900 is 0.92977 and 0.79303 respectively. The b-value (slope) obtained is between 0.5-1 which represents both the diffusion-controlled and surface-controlled capacitive behavior of the electrode. The diffusion-controlled behavior is more dominant in ACJSP-900 than in ACJSP-850 while surface-controlled capacitive behavior is prominent in ACJSP-850.

Separation of capacitive and diffusion-controlled behavior (Dunn's Method):

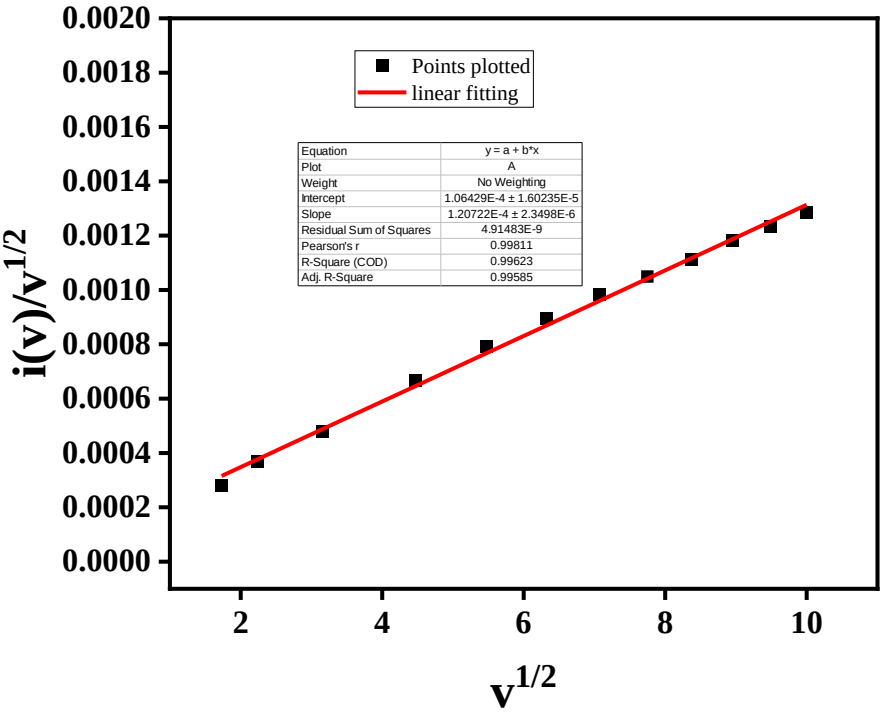

Figure 25 *Surface controlled capacitive behavior of ACJSP-850*

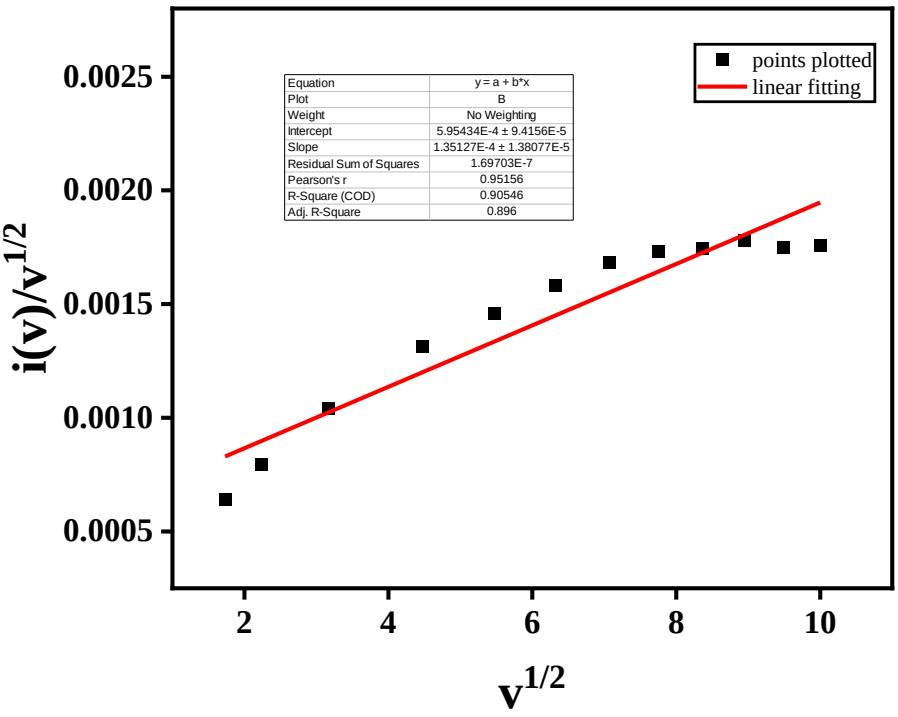

Figure 26 *Diffusion controlled behavior of ACJSP-900*

Figure 25 and Figure 26 show the separation of surface controlled capacitive a diffusion-controlled behavior of prepared ACJSP-850 and ACJPS-900. K_1 and K_2 values of ACJSP-850 are 0.0001207 and 0.0001064 in ACJSP-850. Similarly, K_1 and K_2 values are 0.000135 and 0.000595 for ACJSP-900. Here, at 850 °C $K_1 > K_2$ which validates the surface-controlled capacitive behavior but at 900 °C, $K_2 > K_1$ as a result diffusion-controlled behavior is prominent.

4.2.2 Galvanostatic Charge-Discharge (GCD)

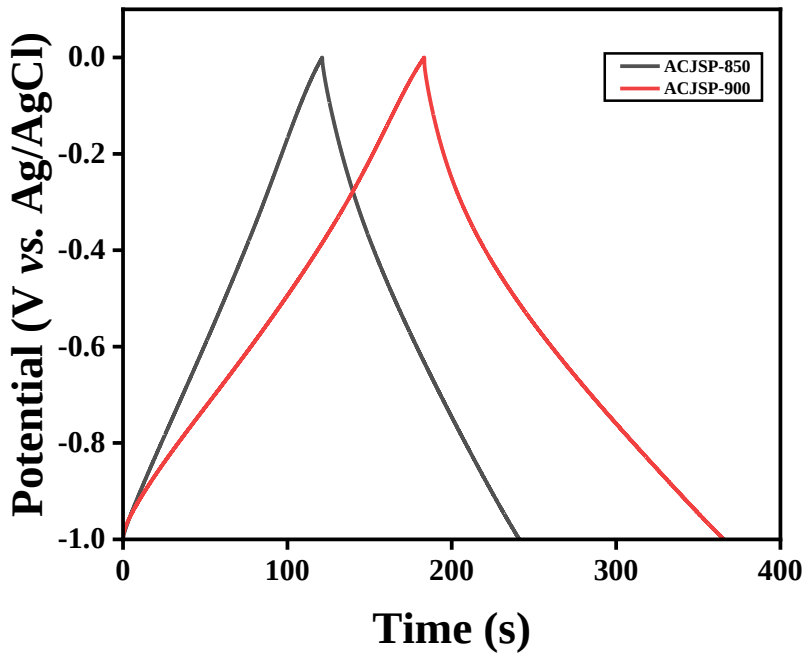

Figure 27 *GCD curve of ACJSP at 1 A* g^{-1}

Figure 27 represents the comparative Galvanostatic Charge-Discharge (GCD) curves of AC from Jacaranda Seed Pods at current density 1 A g^{-1}. AC prepared at higher temperature i.e. 900 °C shows greater charge-discharge time compared to the AC prepared at 850 °C. Further, a nearly symmetric isosceles triangle from the GCD curve supported the formation of an electric double-layer capacitor (EDLC). At 1 A g^{-1} ACJSP-900 showed a specific capacitance of 182 F g^{-1} and ACJSP-850 showed a specific capacitance of 120 F g^{-1}.

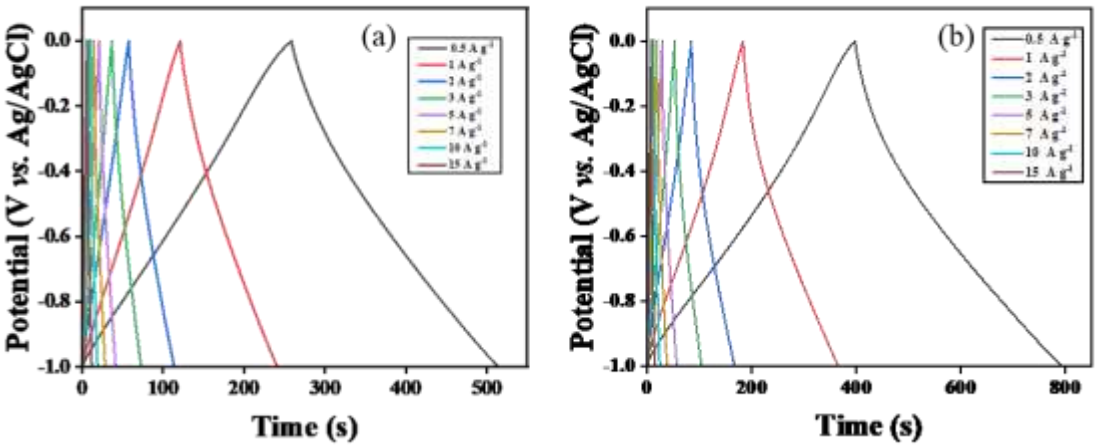

Figure 28 *GCD curve of (a) ACJSP-850 & (b) ACJSP-900 at different current densities*

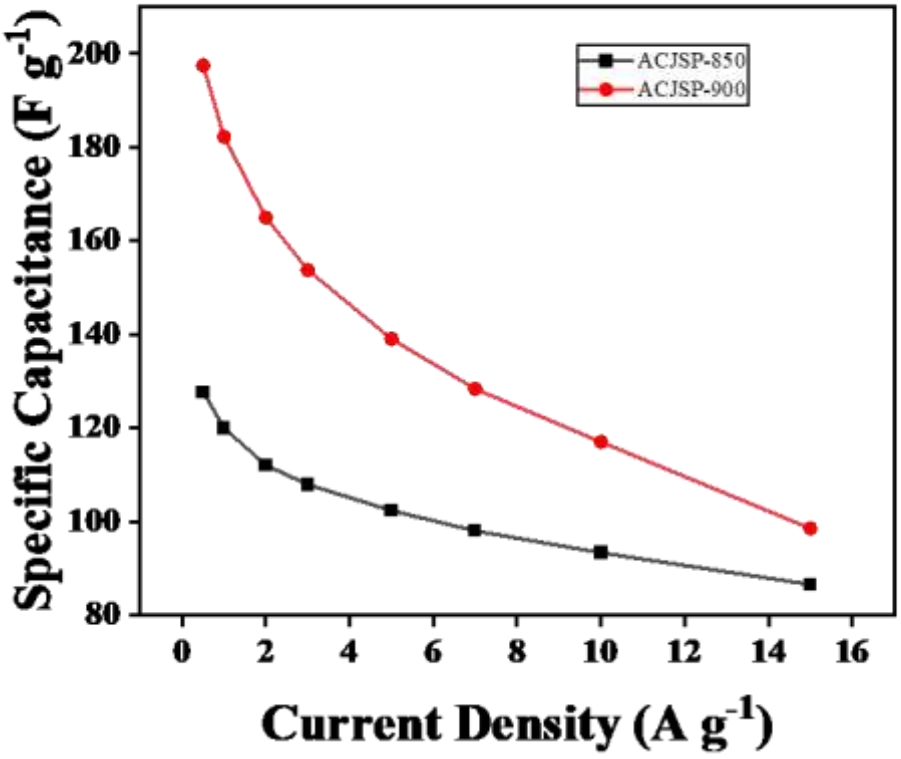

Figure 29 *Specific Capacitance of ACJSP-850 and ACJSP-900 at different current densities*

Similarly, Galvanometric Charge-Discharge (GCD) for the prepared ACJSP-850 & ACJSP-900 were done at different current densities i.e. 0.5 A g^{-1},1 A g^{-1}, 2 A g^{-1}, 3 A g^{-1}, 5 A g^{-1}, 7 A g^{-1}, 10 A g^{-1}, and 15 A g^{-1}, as plotted in Figure 28. The GCD data was then analyzed. The triangular, linearly symmetric nature backed the electrostatic charge storage mechanism denying the possibility of the formation of a pseudo-capacitor or

battery. It also provides insight into the specific capacitance of the activated carbon as showed in Figure 29. ACJSP-850 and ACJSP-900 showed specific capacitance of 120 Fg^{-1} and 182 Fg^{-1} respectively at current density of 1 A g^{-1}. The increase in a current density decreased the specific capacitance due to insufficient ion diffusion at high current density across the electrode-electrolyte interface, higher internal resistance (IR) drop i.e. ohmic losses, and non-ideal electrochemical behavior (Awasthi et al., 2019).

4.2.3 Electrochemical Impedance Spectroscopy (EIS)

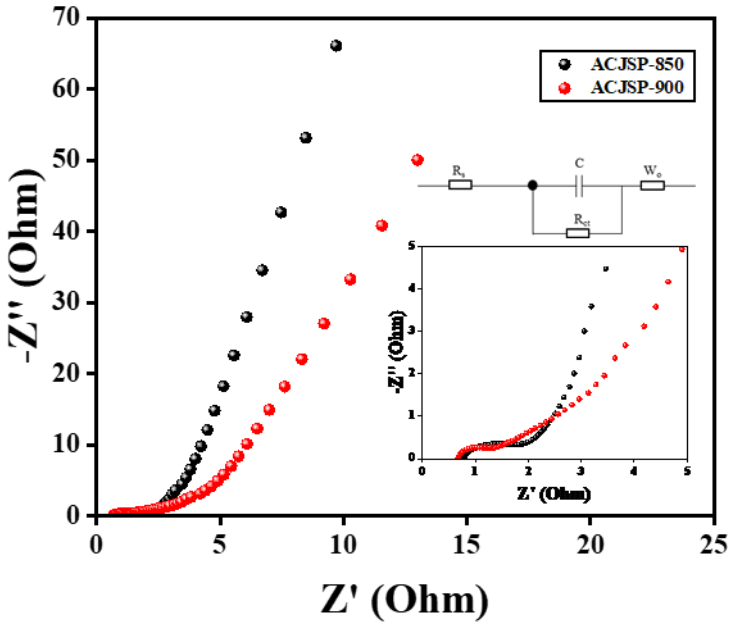

Figure 30 *EIS curve of ACJSP-850 & ACJSP-900*

The provided Electrochemical Impedance Spectroscopy (EIS) plot is a Nyquist plot as shown in Figure 30 that offers insights into the electrochemical characteristics of the material identified as ACJSP-850, and ACJSP-900. The x-axis denotes the resistance (Z') in ohms (Ω), whereas the y-axis indicates the reactance (Z'') in ohms (Ω). The storyline includes solution resistance (R_s), a tiny semicircle in the high-frequency area, representing the charge transfer resistance (R_{ct}) at the interface between the electrode. and electrolyte, and Warburg Impedance represented by W_o. A lower semicircle indicates reduced internal resistance, promoting effective electron transfer. Solution resistance (R_s) is 0.8 Ω, Charge transfer Resistance (R_{ct}) is 0.64 Ω, and Capacitance (C) is 0.00034 F for ACJSP-850. Similarly, for ACJSP-900 R_s is 0.67 Ω , R_{ct} is 0.46 Ω, and C is 0.00020 F. As we progress into the Walburg region, the curve is more pronounced in ACJSP-850 which indicates slower ion diffusion while faster ion diffusion occurs in

ACJSP-900. The almost vertical characteristic of the low-frequency tail suggests electrochemical double-layer capacitance formation with surface capacitive behavior in ACJSP-850. However, more diffusion-based behavior is seen since the curve at low-frequency region is slightly slanted. In general, the EIS plot indicates that ACJSP-900 has minimal charge transfer resistance compared to ACJSP-850. Therefore, it has excellent capacitive response and diffusion-controlled behavior at lower frequencies.

4.2.3 Comparison with other Biomasses Derived Activated Carbon

Table 7: *Comparison with other biomasses derived AC*

Precursor	Temp (°C)	Activating Agent	BET (m^2/g)	Current Density (A/g)	Capacitance (F/g)	References
Orange Peel	800	KOH	2004	0.5	306.6	(Shen et al., 2019)
Bamboo	900	KOH	2221.1	0.5	293	(Zhang et al., 2018)
Pine Saw Dust	900	KOH	2330.89	0.5	175.6	(Quan et al., 2020)
Pinus pinaster Needle	800	H_3PO_4	281.4	0.25	68	(Yumak, 2021)
Walnut Shell	800	H_3PO_4	1956	0.2	46	(Pavlenko et al., 2018)
Baobab Fruit Shell	800	H_3PO_4	911.7	1	355.8	(Mohammed et al., 2019)
Rice Husk	850	KOH	2696	0.1	147	(Liu et al., 2016)
Pinus pinaster Cone	800	H_3PO_4	868.4	0.25	106	(Yumak, 2021)
Jacaranda Seed Pods	900	H_3PO_4	-	1	182	This Work

From Table 7 Jacaranda Seed Pods derived AC shows good performance as an electrode material for EDLC-type supercapacitors due to its diffusion-controlled behavior and higher specific capacitance of 182 F g^{-1} at 900 °C compared to other biomasses. Future work such as nitrogen doping, optimizing activation temperature, and activating agent concentration may enhance the porosity and electrochemical performance of Jacaranda Seed Pods derived AC.

CHAPTER 5: CONCLUSIONS AND RECOMMENDATIONS

5.1 Conclusions

Converting Jacaranda seed pods into activated carbon exemplifies a sustainable and effective method for repurposing agricultural waste for beneficial uses. The activated carbon produced from the JSP shows potential qualities, like large surface area, notable porosity, and increased specific capacitance, making it a competitive electrode material in energy storage devices. At 1 A g^{-1}, ACJSP-900 showed a high specific capacitance of 182 F g^{-1} compared to walnut shells (46 F g^{-1} at 0.2 A g^{-1}), rice husk (147 F g^{-1} at 0.1 A g^{-1}), pine saw dust (175.6 F g^{-1} at 0.5 A g^{-1}), and also ACJSP-850 (120 F g^{-1} at 1 A g^{-1}). The efficient chemical activation and carbonization process, enhanced the material's structural characteristics, allowing it to excel in conductivity (resulting from partial graphitization) and electrochemical performance (due to ion diffusion rate and presence of micro-mesopores). This research emphasizes the possibility of using Jacaranda seed pods as an inexpensive and sustainable source to create activated carbon. Further, this research could aid in utilizing JSP for full-cell testing in two electrode systems through the fabrication of different EDLC type and hybrid type supercapacitors, an alternative for eco-friendly and cost-effective energy storage devices for industrial applications. While promising, the pore size analysis through BET (Brunauer-Emmett-Teller) and BJH (Barrett-Joyner-Halenda), thermal stability, and degradation analysis from Thermogravimetric Analysis (TGA) would provide a comprehensive idea of the material behavior and pore size resulting in optimization of ACJSP.

5.2 Limitations

The research was performed at Pulchowk Campus, Tribhuvan University, Lalitpur Nepal using the existing laboratory facilities. Therefore, the project had some limitations. Raman Spectroscopy, Thermogravimetric Analysis (TGA), BET surface area analysis, and Transmission Electron Microscopy (TEM) were not accessible.

5.3 Recommendations

In order to improve the process of making activated carbon from Jacaranda seed pods, several suggestions can be offered:

- Physical and chemical properties of the activated carbon could be affected by phosphoric acid impregnation ratio, activation temperature, and ramping rate.
- Washing, grinding, sieve analysis, and drying during sample preparation could affect the particle size distribution and influence the results.
- Post-Activation Treatment like washing and drying procedures to eliminate any remaining chemicals and impurities, guarantees the quality and safety of the activated carbon generated.
- Characterization and Testing: Conduct thorough studies to analyze surface area, assess porosity, and test adsorption capacity to assess the activated carbon's performance for particular uses.
- Investigation into Different Methods: Research different activation methods like physical activation or alternative chemical agents to assess efficiency and performance, which may enhance production techniques.

REFERENCES

Abd Mutalib, M., Rahman, M., Othman, M., Ismail, A. F., & Jaafar, J. (2017). Scanning electron microscopy (SEM) and energy-dispersive X-ray (EDX) spectroscopy. In *Membrane characterization* (pp. 161-179). Elsevier.

Abuelnoor, N., AlHajaj, A., Khaleel, M., Vega, L. F., & Abu-Zahra, M. R. (2021). Activated carbons from biomass-based sources for CO2 capture applications. *Chemosphere*, *282*, 131111.

Aguirre-Becerra, H., Pineda-Nieto, S. A., García-Trejo, J. F., Guevara-González, R. G., Feregrino-Pérez, A. A., Álvarez-Mayorga, B. L., & Rivera Pastrana, D. M. (2020). Jacaranda flower (Jacaranda mimosifolia) as an alternative for antioxidant and antimicrobial use. *Heliyon*, *6*(12), e05802. https://doi.org/https://doi.org/10.1016/j.heliyon.2020.e05802

Awasthi, G. P., Bhattarai, D. P., Maharjan, B., Kim, K.-S., Park, C. H., & Kim, C. S. (2019). Synthesis and characterizations of activated carbon from Wisteria sinensis seeds biomass for energy storage applications. *Journal of Industrial and Engineering Chemistry*, *72*, 265-272.

Bakshi, S. D., Sinha, D., & Chowdhury, S. G. (2018). Anisotropic broadening of XRD peaks of α′-Fe: Williamson-Hall and Warren-Averbach analysis using full width at half maximum (FWHM) and integral breadth (IB). *Materials Characterization*, *142*, 144-153.

Balou, S., Babak, S. E., & Priye, A. (2020). Synergistic effect of nitrogen doping and ultra-microporosity on the performance of biomass and microalgae-derived activated carbons for CO2 capture. *ACS Applied Materials & Interfaces*, *12*(38), 42711-42722.

Berthomieu, C., & Hienerwadel, R. (2009). Fourier transform infrared (FTIR) spectroscopy. *Photosynthesis research*, *101*, 157-170.

Bhatla, S. C., & Lal, M. A. (2023). Essential and functional mineral elements. In *Plant physiology, development and metabolism* (pp. 25-49). Springer.

Bhojane, P. (2022). Recent advances and fundamentals of Pseudocapacitors: Materials, mechanism, and its understanding. *Journal of Energy Storage*, *45*, 103654. https://doi.org/https://doi.org/10.1016/j.est.2021.103654

Boundzanga, H. M., Cagnon, B., Roulet, M., de Persis, S., Vautrin-Ul, C., & Bonnamy, S. (2022). Contributions of hemicellulose, cellulose, and lignin to the mass and

the porous characteristics of activated carbons produced from biomass residues by phosphoric acid activation. *Biomass Conversion and Biorefinery*, 1-16.

Brett, C. M., & Brett, O. (1993). Principles, methods, and applications. *Electrochemistry*, *67*(2), 444.

Cagnon, B., Py, X., Guillot, A., Stoeckli, F., & Chambat, G. (2009). Contributions of hemicellulose, cellulose and lignin to the mass and the porous properties of chars and steam activated carbons from various lignocellulosic precursors. *Bioresource Technology*, *100*(1), 292-298.

Chatterjee, D. P., & Nandi, A. K. (2021). A review on the recent advances in hybrid supercapacitors. *Journal of Materials Chemistry A*, *9*(29), 15880-15918.

Chen, W.-H., & Lin, B.-J. (2013). Hydrogen and synthesis gas production from activated carbon and steam via reusing carbon dioxide. *Applied Energy*, *101*, 551-559. https://doi.org/https://doi.org/10.1016/j.apenergy.2012.06.030

Cheng, F., Yang, X., Zhang, S., & Lu, W. (2020). Boosting the supercapacitor performances of activated carbon with carbon nanomaterials. *Journal of Power Sources*, *450*, 227678. https://doi.org/https://doi.org/10.1016/j.jpowsour.2019.227678

Chmiola, J., Yushin, G., Dash, R., & Gogotsi, Y. (2006). Effect of pore size and surface area of carbide derived carbons on specific capacitance. *Journal of Power Sources*, *158*(1), 765-772. https://doi.org/https://doi.org/10.1016/j.jpowsour.2005.09.008

Chmiola, J., Yushin, G., Gogotsi, Y., Portet, C., Simon, P., & Taberna, P.-L. (2006). Anomalous increase in carbon capacitance at pore sizes less than 1 nanometer. *science*, *313*(5794), 1760-1763.

Conway, B. E. (2013). *Electrochemical supercapacitors: scientific fundamentals and technological applications*. Springer Science & Business Media.

Du, Y., Chen, H., Xu, X., Wang, C., Zhou, F., Zeng, Z., Zhang, W., & Li, L. (2020). Surface modification of biomass derived toluene adsorbent: hierarchically porous characterization and heteroatom doped effect. *Microporous and mesoporous materials*, *293*, 109831.

Dutta, A. (2017). Fourier transform infrared spectroscopy. *Spectroscopic methods for nanomaterials characterization*, 73-93.

El Hadrami, A., Ojala, S., & Brahmi, R. (2022). Production of activated carbon with tunable porosity and surface chemistry via chemical activation of hydrochar

with phosphoric acid under oxidizing atmosphere. *Surfaces and Interfaces*, *30*, 101849.

Epp, J. (2016). X-ray diffraction (XRD) techniques for materials characterization. In *Materials characterization using nondestructive evaluation (NDE) methods* (pp. 81-124). Elsevier.

Fang, J., Guo, D., Kang, C., Wan, S., Li, S., Fu, L., Liu, G., & Liu, Q. (2019). Enhanced hetero-elements doping content in biomass waste-derived carbon for high performance supercapacitor. *International Journal of Energy Research*, *43*(14), 8811-8821.

Farghali, M., Osman, A. I., Mohamed, I. M., Chen, Z., Chen, L., Ihara, I., Yap, P.-S., & Rooney, D. W. (2023). Strategies to save energy in the context of the energy crisis: a review. *Environmental Chemistry Letters*, *21*(4), 2003-2039.

Gan, Y. X. (2021). Activated Carbon from Biomass Sustainable Sources. *C*, *7*(2), 39. https://www.mdpi.com/2311-5629/7/2/39

Gayathiri, M., Pulingam, T., Lee, K., & Sudesh, K. (2022). Activated carbon from biomass waste precursors: Factors affecting production and adsorption mechanism. *Chemosphere*, *294*, 133764.

Georgin, J., de O. Salomón, Y. L., Franco, D. S. P., Netto, M. S., Piccilli, D. G. A., Perondi, D., Silva, L. F. O., Foletto, E. L., & Dotto, G. L. (2021). Development of highly porous activated carbon from Jacaranda mimosifolia seed pods for remarkable removal of aqueous-phase ketoprofen. *Journal of Environmental Chemical Engineering*, *9*(4), 105676. https://doi.org/https://doi.org/10.1016/j.jece.2021.105676

Girard, H.-L., Wang, H., d'Entremont, A., & Pilon, L. (2015). Physical interpretation of cyclic voltammetry for hybrid pseudocapacitors. *The Journal of Physical Chemistry C*, *119*(21), 11349-11361.

Głowniak, S., Szczęśniak, B., Choma, J., & Jaroniec, M. (2021). Highly Porous Carbons Synthesized from Tannic Acid via a Combined Mechanochemical Salt-Templating and Mild Activation Strategy. *Molecules*, *26*(7), 1826. https://www.mdpi.com/1420-3049/26/7/1826

Gouy, M. (1910). Sur la constitution de la charge électrique à la surface d'un électrolyte. *J. Phys. Theor. Appl.*, *9*(1), 457-468.

Grahame, D. C. (1947). The electrical double layer and the theory of electrocapillarity. *Chemical reviews*, *41*(3), 441-501.

Harris, P. J., Liu, Z., & Suenaga, K. (2008). Imaging the atomic structure of activated carbon. *Journal of physics: Condensed matter*, *20*(36), 362201.

Heidarinejad, Z., Dehghani, M. H., Heidari, M., Javedan, G., Ali, I., & Sillanpää, M. (2020). Methods for preparation and activation of activated carbon: a review. *Environmental Chemistry Letters*, *18*, 393-415.

Helmholtz, H. v. (1853). Ueber einige Gesetze der Vertheilung elektrischer Ströme in körperlichen Leitern, mit Anwendung auf die thierisch-elektrischen Versuche (Schluss.). *Annalen der Physik*, *165*(7), 353-377.

Holzwarth, U., & Gibson, N. (2011). The Scherrer equation versus the'Debye-Scherrer equation'. *Nature nanotechnology*, *6*(9), 534-534.

Hou, J., Cao, C., Idrees, F., & Ma, X. (2015). Hierarchical porous nitrogen-doped carbon nanosheets derived from silk for ultrahigh-capacity battery anodes and supercapacitors. *ACS nano*, *9*(3), 2556-2564.

Iwanow, M., Gärtner, T., Sieber, V., & König, B. (2020). Activated carbon as catalyst support: precursors, preparation, modification and characterization. *Beilstein Journal of Organic Chemistry*, *16*, 1188-1202. https://doi.org/10.3762/bjoc.16.104

Jiang, C., Yakaboylu, G. A., Yumak, T., Zondlo, J. W., Sabolsky, E. M., & Wang, J. (2020). Activated carbons prepared by indirect and direct CO2 activation of lignocellulosic biomass for supercapacitor electrodes. *Renewable Energy*, *155*, 38-52.

Khan, A., Senthil, R. A., Pan, J., Osman, S., Sun, Y., & Shu, X. (2020). A new biomass derived rod-like porous carbon from tea-waste as inexpensive and sustainable energy material for advanced supercapacitor application. *Electrochimica acta*, *335*, 135588.

Kumar, R., Sahoo, S., Joanni, E., Singh, R. K., Maegawa, K., Tan, W. K., Kawamura, G., Kar, K. K., & Matsuda, A. (2020). Heteroatom doped graphene engineering for energy storage and conversion. *Materials Today*, *39*, 47-65.

Laheäär, A., Przygocki, P., Abbas, Q., & Béguin, F. (2015). Appropriate methods for evaluating the efficiency and capacitive behavior of different types of supercapacitors. *Electrochemistry Communications*, *60*, 21-25.

Li, W., Ding, Y., Zhang, W., Shu, Y., Zhang, L., Yang, F., & Shen, Y. (2016). Lignocellulosic biomass for ethanol production and preparation of activated

carbon applied for supercapacitor. *Journal of the Taiwan Institute of Chemical Engineers*, *64*, 166-172.

Li, X., Ding, Y., Zhang, H., He, T., Hao, J., Wu, J., Wu, Y., & Bai, H. (2024). Pine sawdust derived ultra-high specific surface area activated carbon: Towards high-performance hydrogen storage and supercapacitors. *International Journal of Hydrogen Energy*, *84*, 623-633.

Li, Y., Zhang, X., Yang, R., Li, G., & Hu, C. (2015). The role of H 3 PO 4 in the preparation of activated carbon from NaOH-treated rice husk residue. *RSC advances*, *5*(41), 32626-32636.

Libich, J., Máca, J., Vondrák, J., Čech, O., & Sedlaříková, M. (2018). Supercapacitors: Properties and applications. *Journal of Energy Storage*, *17*, 224-227.

Liu, D., Zhang, W., Lin, H., Li, Y., Lu, H., & Wang, Y. (2016). A green technology for the preparation of high capacitance rice husk-based activated carbon. *Journal of cleaner production*, *112*, 1190-1198.

Liu, H., Song, H., Chen, X., Zhang, S., Zhou, J., & Ma, Z. (2015). Effects of nitrogen- and oxygen-containing functional groups of activated carbon nanotubes on the electrochemical performance in supercapacitors. *Journal of Power Sources*, *285*, 303-309.

Magar, H. S., Hassan, R. Y., & Mulchandani, A. (2021). Electrochemical impedance spectroscopy (EIS): Principles, construction, and biosensing applications. *Sensors*, *21*(19), 6578.

Mohammed, A. A., Chen, C., & Zhu, Z. (2019). Low-cost, high-performance supercapacitor based on activated carbon electrode materials derived from baobab fruit shells. *Journal of colloid and interface science*, *538*, 308-319.

Molina-Sabio, M., Gonzalez, M. T., Rodriguez-Reinoso, F., & Sepúlveda-Escribano, A. (1996). Effect of steam and carbon dioxide activation in the micropore size distribution of activated carbon. *Carbon*, *34*(4), 505-509. https://doi.org/https://doi.org/10.1016/0008-6223(96)00006-1

Morales-Herrera, V. A., Quintero-Álvarez, F. G., Mendoza-Castillo, D. I., Reynel-Ávila, H. E., Aguayo-Villarreal, I. A., Landin-Sandoval, V. J., & Bonilla-Petriciolet, A. (2024). Assessment and modeling of mercury adsorption on carbon-based adsorbents prepared from Jacaranda mimosifolia and guava biomass via pyrolysis and hydrothermal carbonization. *Water Practice & Technology*, *19*(4), 1162-1176.

Mukhiya, T., Dahal, B., Ojha, G. P., Kang, D., Kim, T., Chae, S.-H., Muthurasu, A., & Kim, H. Y. (2019). Engineering nanohaired 3D cobalt hydroxide wheels in electrospun carbon nanofibers for high-performance supercapacitors. *Chemical Engineering Journal*, *361*, 1225-1234.

Mukhiya, T., Muthurasu, A., Tiwari, A. P., Chhetri, K., Chae, S.-H., Kim, H., Dahal, B., Lee, B. M., & Kim, H. Y. (2021). Integrating the essence of a metal–organic framework with electrospinning: a new approach for making a metal nanoparticle confined N-doped carbon nanotubes/porous carbon nanofibrous membrane for energy storage and conversion. *ACS Applied Materials & Interfaces*, *13*(20), 23732-23742.

Nandee, R., Chowdhury, M. A., Hossain, N., Rana, M. M., Mobarak, M. H., & Khandaker, M. R. (2024). Surface topography and surface morphology of graphene nanocomposite by FESEM, EDX and AFM analysis. *Nano-Structures & Nano-Objects*, *38*, 101170.

Neme, I., Gonfa, G., & Masi, C. (2022). Activated carbon from biomass precursors using phosphoric acid: A review. *Heliyon*, *8*(12).

Niya, S. R., & Andrews, J. (2022). On charge distribution and storage in porous conductive carbon structure. *Electrochimica Acta*, *402*, 139534.

Nor, N. M., Lau, L. C., Lee, K. T., & Mohamed, A. R. (2013). Synthesis of activated carbon from lignocellulosic biomass and its applications in air pollution control—a review. *Journal of Environmental Chemical Engineering*, *1*(4), 658-666.

Owsianiak, M., Lindhjem, H., Cornelissen, G., Hale, S. E., Sørmo, E., & Sparrevik, M. (2021). Environmental and economic impacts of biochar production and agricultural use in six developing and middle-income countries. *Science of the total environment*, *755*, 142455.

Pandolfo, A. G., & Hollenkamp, A. F. (2006). Carbon properties and their role in supercapacitors. *Journal of power sources*, *157*(1), 11-27.

Pavlenko, V., Abbas, Q., Przygocki, P., Kon'kova, T., Supiyeva, Z., Abeykoon, N., Prikhodko, N., Bijsenbayev, M., Kurbatov, A., & Lesbayev, B. (2018). Temperature dependent characteristics of activated carbons from walnut shells for improved supercapacitor performance. *Eurasian Chemico-Technological Journal*, *20*(2), 99-105.

Quan, C., Su, R., & Gao, N. (2020). Preparation of activated biomass carbon from pine sawdust for supercapacitor and CO2 capture. *International Journal of Energy Research*, *44*(6), 4335-4351.

Rodríguez-Reinoso, F., & Molina-Sabio, M. (1992). Activated carbons from lignocellulosic materials by chemical and/or physical activation: an overview. *Carbon*, *30*(7), 1111-1118. https://doi.org/https://doi.org/10.1016/0008-6223(92)90143-K

Saini, S., Chand, P., & Joshi, A. (2021). Biomass derived carbon for supercapacitor applications. *Journal of Energy Storage*, *39*, 102646.

Salanne, M., Rotenberg, B., Naoi, K., Kaneko, K., Taberna, P.-L., Grey, C. P., Dunn, B., & Simon, P. (2016). Efficient storage mechanisms for building better supercapacitors. *Nature Energy*, *1*(6), 1-10.

Shen, H., Xia, X., Ouyang, Y., Jiao, X., Mutahir, S., Mandler, D., & Hao, Q. (2019). Preparation of biomass-based porous carbons with high specific capacitance for applications in supercapacitors. *ChemElectroChem*, *6*(14), 3599-3605.

Simon, P., & Gogotsi, Y. (2008). Materials for electrochemical capacitors. *Nature materials*, *7*(11), 845-854.

Sinha, D., & Tandon, P. K. (2020). An overview of nitrogen, phosphorus and potassium: Key players of nutrition process in plants. *Sustainable solutions for elemental deficiency and excess in crop plants*, 85-117.

Sivachidambaram, M., Vijaya, J. J., Niketha, K., Kennedy, L. J., Elanthamilan, E., & Merlin, J. P. (2019). Electrochemical studies on tamarindus indica fruit shell bio-waste derived nanoporous activated carbons for supercapacitor applications. *Journal of Nanoscience and Nanotechnology*, *19*(6), 3388-3397.

Srirangan, K., Akawi, L., Moo-Young, M., & Chou, C. P. (2012). Towards sustainable production of clean energy carriers from biomass resources. *Applied energy*, *100*, 172-186.

Stern, O. (1924). Zur theorie der elektrolytischen doppelschicht. *Zeitschrift für Elektrochemie und angewandte physikalische Chemie*, *30*(21-22), 508-516.

Suárez-Garcıa, F., Martınez-Alonso, A., & Tascón, J. D. (2002). Pyrolysis of apple pulp: chemical activation with phosphoric acid. *Journal of Analytical and Applied Pyrolysis*, *63*(2), 283-301.

Tiwari, P., Jaiswal, J., & Chandra, R. (2019). Hierarchal growth of MoS2@ CNT heterostructure for all solid state symmetric supercapacitor: Insights into the surface science and storage mechanism. *Electrochimica Acta*, *324*, 134767.

Treviño-Cordero, H., Juárez-Aguilar, L., Mendoza-Castillo, D., Hernández-Montoya, V., Bonilla-Petriciolet, A., & Montes-Morán, M. (2013). Synthesis and adsorption properties of activated carbons from biomass of Prunus domestica and Jacaranda mimosifolia for the removal of heavy metals and dyes from water. *Industrial Crops and Products*, *42*, 315-323.

Ullah, S., Shah, S. S. A., Altaf, M., Hossain, I., El Sayed, M. E., Kallel, M., El-Bahy, Z. M., Rehman, A. u., Najam, T., & Nazir, M. A. (2024). Activated carbon derived from biomass for wastewater treatment: Synthesis, application and future challenges. *Journal of Analytical and Applied Pyrolysis*, *179*, 106480. https://doi.org/https://doi.org/10.1016/j.jaap.2024.106480

Valdés-Rodríguez, E., Mendoza-Castillo, D., Reynel-Ávila, H., Aguayo-Villarreal, I., & Bonilla-Petriciolet, A. (2022). Activated carbon manufacturing via alternative Mexican lignocellulosic biomass and their application in water treatment: Preparation conditions, surface chemistry analysis and heavy metal adsorption properties. *Chemical engineering research and design*, *187*, 9-26.

Wang, Q., Su, J., Chen, H., Wang, D., Tian, X., Zhang, Y., Feng, X., Wang, S., Li, J., & Jin, H. (2022). Highly conductive nitrogen-doped sp2/sp3 hybrid carbon as a conductor-free charge storage host. *Advanced Functional Materials*, *32*(51), 2209201.

Ward, K. R., Lawrence, N. S., Hartshorne, R. S., & Compton, R. G. (2012). The theory of cyclic voltammetry of electrochemically heterogeneous surfaces: comparison of different models for surface geometry and applications to highly ordered pyrolytic graphite. *Physical chemistry chemical physics : PCCP*, *14*(20), 7264-7275. https://doi.org/10.1039/c2cp40412e

Xu, Y. J., Weinberg, G., Liu, X., Timpe, O., Schlögl, R., & Su, D. S. (2008). Nanoarchitecturing of activated carbon: facile strategy for chemical functionalization of the surface of activated carbon. *Advanced Functional Materials*, *18*(22), 3613-3619.

Yu, M., Han, Y., Li, J., & Wang, L. (2017). CO2-activated porous carbon derived from cattail biomass for removal of malachite green dye and application as supercapacitors. *Chemical Engineering Journal*, *317*, 493-502.

Yumak, T. (2021). Surface characteristics and electrochemical properties of activated carbon obtained from different parts of Pinus pinaster. *Colloids and Surfaces A: Physicochemical and Engineering Aspects*, *625*, 126982.

Zhang, G., Chen, Y., Chen, Y., & Guo, H. (2018). Activated biomass carbon made from bamboo as electrode material for supercapacitors. *Materials Research Bulletin*, *102*, 391-398.

Zhang, L. L., & Zhao, X. (2009). Carbon-based materials as supercapacitor electrodes. *Chemical society reviews*, *38*(9), 2520-2531.

Zhang, S., Zheng, M., Tang, Y., Zang, R., Zhang, X., Huang, X., Chen, Y., Yamauchi, Y., Kaskel, S., & Pang, H. (2022). Understanding synthesis–structure–performance correlations of nanoarchitectured activated carbons for electrochemical applications and carbon capture. *Advanced Functional Materials*, *32*(40), 2204714.

Zhao, X., & Liu, Y. (2021). Origin of Selective Production of Hydrogen Peroxide by Electrochemical Oxygen Reduction. *Journal of the American Chemical Society*, *143*(25), 9423-9428. https://doi.org/10.1021/jacs.1c02186

Zou, Z., Liu, T., & Jiang, C. (2019). Highly mesoporous carbon flakes derived from a tubular biomass for high power electrochemical energy storage in organic electrolyte. *Materials Chemistry and Physics*, *223*, 16-23.

Activated Carbon from Jacaranda Seed Pods for Energy Storage

Ashman Karki [a], *Bipana Ojha Khatri* [b],
Rajesh Shrestha [c], *Purnima Mulmi* [d], *Tanka Mukhiya* [e*]

Abstract:

Activated carbon (AC) is a multifunctional material widely used in various applications such as energy storage, water purification, skincare, and other industrial operations. Locally available biowaste is a low-cost resource for AC. This study focuses on synthesizing AC from Jacaranda Seed Pods (JSP) - lignocellulosic biomass and testing its electrochemical properties. JSP powder was activated using phosphoric acid at 850 °C. As-prepared AC was characterized via Field Emission Scanning Electron Microscopy (FESEM) and Fourier transform Infrared Spectroscopy (FTIR). Additionally, electrochemical properties for energy storage were tested with Cyclic Voltammetry (CV) and Galvanostatic Charging Discharging (GCD). The FESEM image verified the prepared activated carbon is highly porous. The electrochemical study shows that as-prepared AC exhibits good energy storage capacity. Hence, activated carbon prepared from JSP could be a promising candidate for energy storage applications.

Keywords:

Activated carbon, biowaste, Jacaranda, electrochemical study, energy storage

[a, b, c, d, e] *Department of Applied Sciences and Chemical Engineering, Pulchowk Campus, IOE, Tribhuvan University, Nepal*

[e*] tanka.mukhiya@pcampus.edu.np

7% Overall Similarity

The combined total of all matches, including overlapping sources, for each database.

Filtered from the Report

- Bibliography
- Quoted Text
- Small Matches (less than 10 words)

Match Groups

44 Not Cited or Quoted 7%
Matches with neither in-text citation nor quotation marks

6 Missing Quotations 1%
Matches that are still very similar to source material

0 Missing Citation 0%
Matches that have quotation marks, but no in-text citation

0 Cited and Quoted 0%
Matches with in-text citation present, but no quotation marks

Top Sources

6% Internet sources
4% Publications
0% Submitted works (Student Papers)

Integrity Flags

0 Integrity Flags for Review

No suspicious text manipulations found.

Our system's algorithms look deeply at a document for any inconsistencies that would set it apart from a normal submission. If we notice something strange, we flag it for you to review.

A Flag is not necessarily an indicator of a problem. However, we'd recommend you focus your attention there for further review.